Assessment of the influence of natural thermal cycles on dolomitic limestone rock columns: A 10-year monitoring study

Muriel Gasc-Barbier, Véronique Merrien-Soukatchoff, Vincent Krzewinski, Pierre Azemard, Jean-Luc Genois

▶ **To cite this version:**

Muriel Gasc-Barbier, Véronique Merrien-Soukatchoff, Vincent Krzewinski, Pierre Azemard, Jean-Luc Genois. Assessment of the influence of natural thermal cycles on dolomitic limestone rock columns: A 10-year monitoring study. Geomorphology, 2024, 464, pp.109353. 10.1016/j.geomorph.2024.109353 . hal-04679073

HAL Id: hal-04679073
https://cnam.hal.science/hal-04679073v1

Submitted on 8 Oct 2024

HAL is a multi-disciplinary open access archive for the deposit and dissemination of scientific research documents, whether they are published or not. The documents may come from teaching and research institutions in France or abroad, or from public or private research centers.

L'archive ouverte pluridisciplinaire **HAL**, est destinée au dépôt et à la diffusion de documents scientifiques de niveau recherche, publiés ou non, émanant des établissements d'enseignement et de recherche français ou étrangers, des laboratoires publics ou privés.

Assessment of the influence of natural thermal cycles on dolomitic limestone rock columns: a 10-year monitoring study

1 INTRODUCTION

Geomorphology is focused on the explanation of the surface of the Earth. As explained by (Hall et al., 2012), "the Earth's landforms and landscapes express the integration of the balance between internal and external forces influencing that surface, as modulated by both a unique local history and the surface material". Moreover, these authors precise that this balance is dynamic and that weathering is a fundamental topic as it is the "initial or primary expression of the transition from domination of material by internal forces to modification by external forces". Therefore the action of weathering is significant in landscape evolution (Gasc-Barbier et al., 2021).

Rock fracturing plays a key role in the process of weathering (Eppes, 2022), because in the one hand it will increase the weathering as cracks are predisposing factors and, in the other hand, it is the consequence of weathering. Cracks modify the mechanical, chemical, and hydrological properties of the rock, and rock fracturing is the first step of erosion processes as it enables the development of isolated debris. When considering the failure of steep rock slopes, different agents of weathering should be considered as triggering factors, such as freezing (Deprez et al., 2020; Frayssines and Hantz, 2006; Matsuoka, 2008, 2001), rain (Balducci, 2007; Bernardie et al., 2014; Bezak and Mikoš, 2021; Chigira, 2009; Galeandro et al., 2014; Iverson, 2000; Regmi et al., 2013) or thermal variations (Alcaíno-Olivares et al., 2023; Breytenbach, 2022; Collins and Stock, 2016; Eppes et al., 2010; Eppes and Griffing, 2010; Eppes and Keanini, 2017; Gunzburger et al., 2005; Hall, 1999; Hall and Thorn, 2014; Marmoni et al., 2020; Mufundirwa et al., 2011; Ravaji et al., 2019; Vargas et al., 2004). More specifically, the influence of temperature as one of the agents of the alteration has been drawn due to several events where other causes could not be invoked (Collins et al., 2018; Gasc-Barbier et al., 2015; Gunzburger and Merrien-Soukatchoff, 2011; Vargas et al., 2009).

Merrien-Soukatchoff and Gasc-Barbier, (2023) have recently reviewed the accumulated knowledge on the effect of positive temperature cycles on rock slope stability. They offered a comprehensive summary on the site investigations conducted in the last 35 years, focusing on the effect of natural thermal cycles simultaneously at the surface and in the rock mass. Temperature is mostly measured at the surface (Alcaíno-Olivares et al., 2023; Guerin et al., 2021; Marmoni et al., 2020; McKay et al., 2009) but also in the rock mass (Breytenbach, 2022; Racek et al., 2021) up to 6 m (Gasc-Barbier et al., 2021). Displacements are sometimes registered (Bièvre et al., 2018; Guerin et al., 2021; Gunzburger et al., 2005; Krähenbühl, 2004) but in most cases it is fracture openings and closures that are recorded (Alcaíno-Olivares et al., 2023; Cloutier et al., 2015; Gischig et al., 2010; Grøneng et al., 2011; Mufundirwa et al., 2011; Racek et al., 2023).

Such thermomechanical measurements were observed in a wide range of lithologies (gneissic rock (Grøneng et al., 2011; Gunzburger et al., 2005; Krähenbühl, 2004), granite (Collins et al., 2018; Guerin et al., 2021) or different types of limestone (Bakun-Mazor et al., 2013; Gasc-Barbier et al., 2021; Marmoni et al., 2020; Taboada et al., 2017; Vlcko et al., 2009)) and climatic conditions (desertic areas, temperate climate, etc.). Different approaches to data processing and modelling can be used: in some cases, theoretical models are focused on rock mass deformations that result from continuous models of rock deformations, neglecting the presence of joints. Other approaches neglect the transient state of the environmental fluctuations.

This preprint research paper has not been peer reviewed. Electronic copy available at: https://ssrn.com/abstract=4743392

Nevertheless, all authors agree on the importance of data acquisition during long timeframes to better assess the time-dependent behaviour of the rock mass. As long-time measurements are rare, the effect of climatic factors on rock weathering remains relatively poorly understood in the long term, especially if we try to translate it into thermomechanical constitutive laws. As mentioned, numerous papers show the influence of temperature, but most of the sites under study are monitored during small periods, from a few days to a year. Those time laps are enough to identify some thermomechanical behaviour but are not long enough to completely characterise them especially when the mechanisms evolve with time. In the case of les *chandelles de l'Escalette*, eleven fissurometers with temperature measurements were positioned along 50-meter-high dolomitic columns and were monitored for 10 years. It enables us to depict the long-term interaction between thermal solicitation and displacements along fractures and separated rock masses.

2 GEOMORPHOLOGICAL AND GEOLOGICAL SETTINGS

2.1 General description

Les chandelles de l'Escalette are located in the south of France (see insert in Figure 1) just above an important highway and above the south heads of a tunnel (Figure 1). They are located at the bottom of a *dead-end* valley of the Lergue River on the southern edge of the Larzac plateau. A simplified geological log is given on the right part of Figure 1a, Figure 1b presents a top view of the site and Figure 1c is a geological map of the area (caution: scales are not the same).

The rock columns are Bathonian (J2b[1]) dolomitic limestone of approximately 60 m high. They lie on about 30 m of infra-Bathonian (J2a), that are sub-lithographic limestones in small banks and fetid marls with lignite debris around 30-m thick. This level forms the smoother slope separating the two stiff cliffs (see Figure 1a). The underlying Bajocian (J1b) is characterised by a rather massive light beige saccharoidal dolomite in large banks. Finally, a small thickness of Aalanian (lJ0-1) marl -interlace limestone in small banks outcrops at the base of the topography. Dolomite from Bathonian and Bajocian give steep cliffs whereas infra-Bathonian and Aalanian limestone leads to gentler slopes. The local dip of the layers is about 5° to 6° to the north.

Wider, the southern edge of the Larzac plateau presents a relatively simple tabular and sub horizontal structure made of Bathonian dolomite (light brown in fig 1c). The blind valley cut by the Lergue River where the *chandelles* are located is easily observed on the geological map. From a structural point of view, a major fault is located just at the north of the tunnel. An aerial photointerpretation has shown a fairly dense fractures network oriented N30, N70, N100, N130, N160. These directions are readable in the morphology of the cliffs.

The nearest weather station was set up at Caylar in 2007 (https://donneespubliques.meteofrance.fr/?fond=contenu&id_contenu=37 - ID 34064003). This small village is located on the Larzac plateau, about 5 km at the North of the *Chandelles*. French climate classification made by (Joly et al. 2010) describe an Altered Mediterranean Climate: the average annual temperature is high, with a small number of cold days and between 15 and 23 hot days per year. Inter-annual variability in July temperatures is minimal: summer is repeatedly hot from one year to the other. Annual rainfall is average (800-950 mm) but is not evenly distributed.

[1] J1b, lJ0-1, J2b, J2a are geological denominations that can be seen on Figure 1c

Preprint not peer reviewed

This preprint research paper has not been peer reviewed. Electronic copy available at: https://ssrn.com/abstract=4743392

a

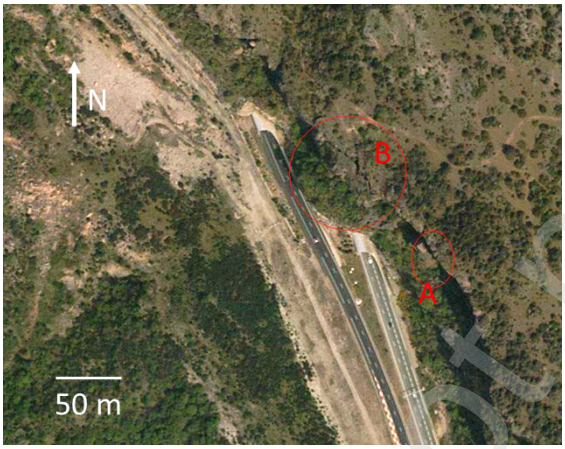

b

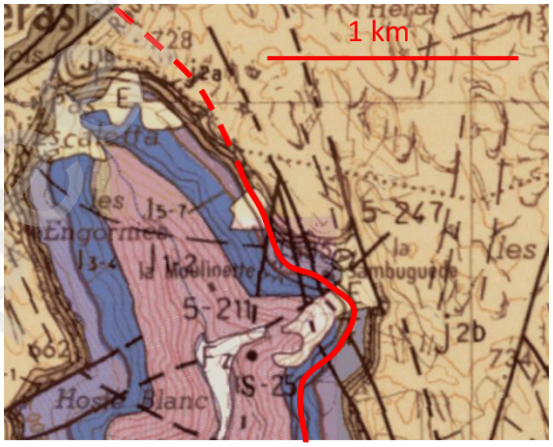

C

Figure 1: Location of the site and geological clues. a- general view of the columns and simplified geological interpretation b-Top view of the site - red circles show the large fractures that separate the columns from the cliff; c- Geological map of the area, the highway is in red, the tunnel is in dotted line.

2.2 Description of the columns

2.2.1 Description of column A

Column A (see Figure 1a) is almost pyramidal and culminates at 659 m; its base is estimated at 622 m according to the lowest point of the western face. Thus, the height of the column A is about 37 m. It should be noted that mining in 1993 (during road works) reduced its height by around 15 m. An estimation gives the roof of the infra-Bartonian between 619 and 621 m, which means that the column is entirely composed of the dolomitic Bathonian. More precisely, its top is about 7 m thick and 10 m long and its base is about 12 m thick and 30 m long. The back of the column is a well-defined crack oriented N150, with an opening ranging from 1.3 m to 1.55 m. The bottom of the back crack is covered with earthy soil, with a large block in the centre. The column is very massive. The volume of the column is about 5000 m^3. Its gravity

This preprint research paper has not been peer reviewed. Electronic copy available at: https://ssrn.com/abstract=4743392

centre is anticipated at about 634 m high, that is 12 m above the base, 4.8 m of the back crack and 7 m behind the front face.

2.2.2 Description of column B

This column has a parallelepipedal shape. It culminates between 661 m and 665 m, its base is estimated between 612 m and 620 m. Its height is about 45 to 49 m. At the top it has a trapezoidal section of 80 and 45 m in length for a width of about 13 m. The area is almost identical from the base to 645 m high, then decreases slightly on the north side. Its total volume is about 34 000 m3.

The global centre of gravity is estimated at 637 m (20 / 25 m above the base); at about 8.2 m from the front face and 8.0 m from the back face, and 37.7 m from the foot of the fissure in the South (40 m from the foot of the fissure in the North).

This large column is divided into 3 main masses (see Figure 2a).

- In the North a small column, B_1 is about 15 m long and 1 to 11 m thick for a height of 40 m.
- In the centre, the main mass B_2 is 55 m long and 12 to 15 m thick, for a height of 50 m. A crack well defined delimited spalling C (see Figure 2b)
- In the south a much smaller column B_3 is about 15 m long and 6 m thick for a height of 50m (see Figure 2b).

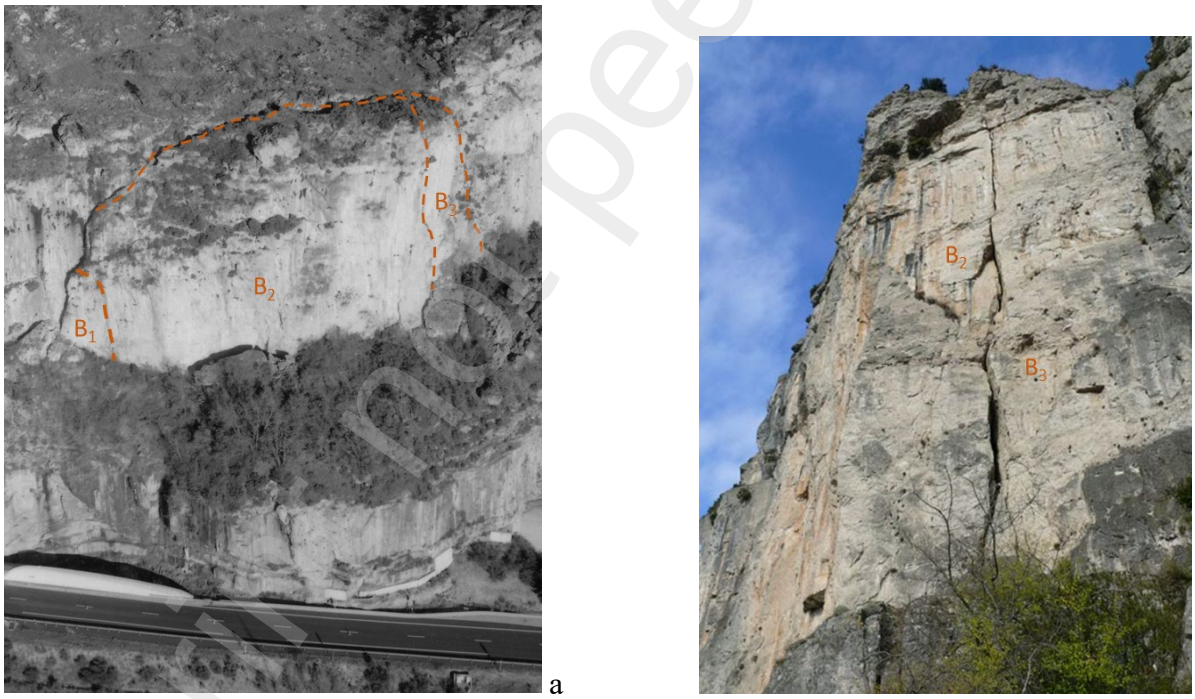

a b

Figure 2: Views of column B. a- global view from helicopter, b- lateral view from the intermediate ridge. B_1 is about 15 m long and 1 to 11 m thick and 40 m high, B_2 is 55 m long and 12 to 15 m thick, for a height of 50 m, and B_3 is about 15 m long and 6 m thick.

2.3 Monitoring devices

The purpose of the monitoring device was not to precisely catch the thermomechanical processes. The aim was to understand if and how the column moved and assess the associated hazard on the area and more specifically on the highway, but thermomechanical behaviour was

Preprint not peer reviewed

This preprint research paper has not been peer reviewed. Electronic copy available at: https://ssrn.com/abstract=4743392

found. The monitoring device is composed of eleven fissurometers, corresponding to the red points in Figure 3a, and also positioned on the simplified diagram represented in Figure 3b. Along each important fracture (see Figure 2) two pairs of sensors were located, one at the bottom (B sensors), one near the top (H sensors). More precisely: H1 and B2 are located between column A and the cliff; H3 and B4 are located between column B_3 and the cliff; H5 and B6 between columns B_2 and B_3; H7 and H9 are located between column B_2 and the cliff and finally B8, V8 and B10 are located between column B_1 and the cliff (at the bottom of the large fracture), see Figure 3b.

a

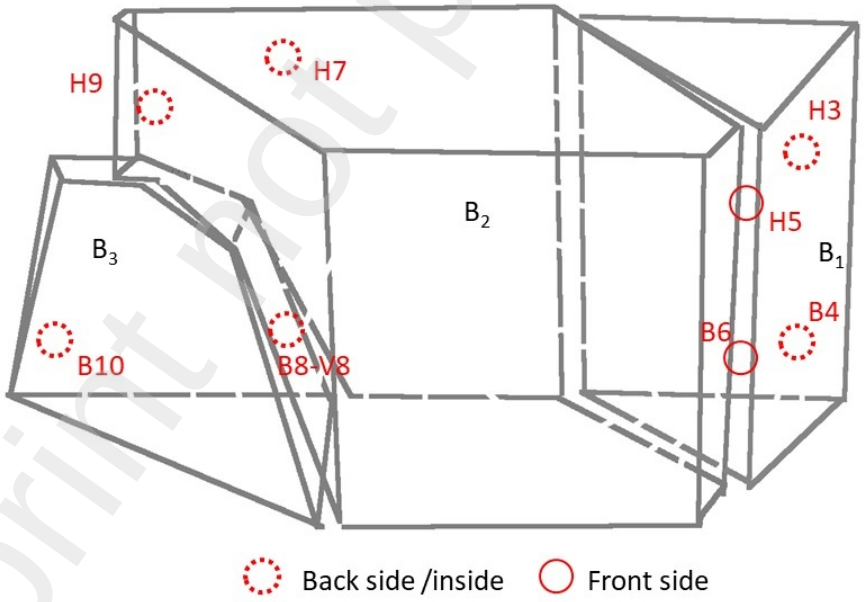

b

Preprint not peer reviewed

This preprint research paper has not been peer reviewed. Electronic copy available at: https://ssrn.com/abstract=4743392

c

d

Figure 3: Instrumentation. a- general view, b, simplified diagram of the position of sensor in columns B, c, sensor H3 set-up, d- sensor B4

All fissurometers are horizontal, expect V8 which is vertical and located near B8 (only one red point corresponding to both B8 and V8 is displayed in Figure 3). Temperature is measured near each fissurometer.

Apart from H5 and B6, all the sensors are positioned on the back side of the columns, in screw-to-screw of the cliff (H3, B4, H9, B10), or inside, between parts of column B (H7, B8, V8). This point is important when considering the influence of temperature on the displacement and especially because they are not exposed to sunlight.

Figure 3d gives an example of a fissurometer in place and Figure 3c shows the set-up. Photos of all fissurometers are displayed in appendix 1.

3 RESULTS

Temperature and displacement recording began in November 2012 (on the 7th). A measure is taken every hour, except for few periods due to measurement devices shutdown, depending on the sensors. Most fissurometers are still recording even if, after six or seven years of records, we observed more and more noise and some unexplained steps. Data up to October 2022 are available on sensors H3, B4, H5 and B6. Only part of the data (up to 2018 or 2021) is available on the other sensors.

3.1 Temperature recording

3.1.1 General observations

Figure 4 presents temperature recording from November 2012 to October 2022 in H5 sensors. To make the data more readable, we only plotted the average weekly temperature (dots) and weekly maximum and minimum (error bar in blue). The seasonality is obvious and the 10 years can be recognized in Figure 11 All temperature curves are given in appendix 2, presented 2 by 2 on the same graph (H and B for the same global location).

Preprint not peer reviewed

This preprint research paper has not been peer reviewed. Electronic copy available at: https://ssrn.com/abstract=4743392

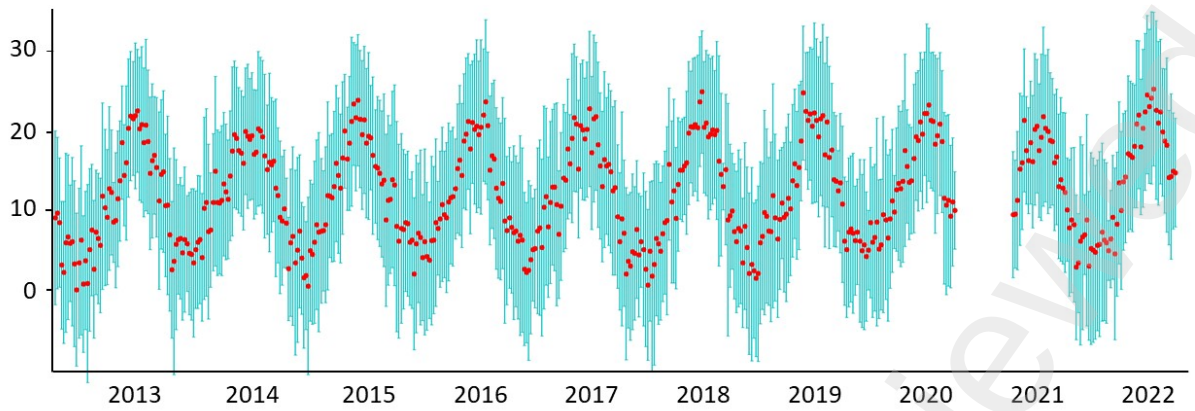

Figure 4: 10 years of temperature recordings on H5 sensor: dots: average weekly temperature, error bar: weekly minimum and maximum

The temperatures recorded are broadly the same in all the sensors, but a closer look reveals some local variations. Temperatures are more widely dispersed in the upper sensors than in the lower ones. (see also Figure 6).

Table 1 presents minimum and maximum temperature recorded for each sensor. The maximum temperature over the period is 37.67°C obtain on sensor H7 the 2017-06-17 at 8 p.m. On the 2nd of August 2018 at 9 p.m., we recorded the maximum temperature value for sensors B8 (36.93°C), H9 (36.92°C) and B10 (36.94°C). The minimum temperature over the period is -11.98°C obtained on sensor H3 the 2018-02-27 at 10 a.m. The same day, at the same hour, we have recorded the minimum values of B4 (-10.64°C), H5 (-9.08°C) and B6 (-11°C).

Max daily amplitude over the period is 30.18°C obtain on sensor B2 on the 03/12/2013 then 27.6 obtained on B6 on the 2017/01/19. The minimum daily amplitude is between 0°C and 1°C. It is obtained during the winter months, mostly in December, with no sunshine.

Table 1: Minimum and maximum temperature and maximum daily amplitude recorded.

	Min		Max		Amplitude max	
	val	date	val	date	val	date
H1	-8.8°C	2018/02/27	33.84°C	2022/08/04	24.15°C	2022/07/31
B2	-6.81	2017/11/26	40.65°C	2016/09/11	27.75°C	2017/03/10
H3	-11.98°C	2018/02/27	39.21°C	2019/06/28	22.28°C	2020/07/12
B4	-10.64°C	2018/02/27	35.14°C	2020/08/08	19.3°C	2017/10/04
H5	-9.08°C	2018/02/27	37.74°C	2022/08/02	24.11°C	2013/12/03
B6	-11°C	2018/02/27	39.6°C	2022/08/07	28.48°C	2022/09/18
H7	-9.07°C	2013/01/18	38.46°C	2017/06/17	24.52°C	2016/08/07
B8	-5.79°C	2017/10/29	38.17°C	2022/08/07	14.83°C	2018/04/015
H9	-9.2°C	2018/02/27	38.2°C	2022/08/07	18.65°C	2014/03/17
B10	-9.92°C	2018/02/27	38.18°C	2022/08/07	21.24°C	2017/08/21

Figure 5 and Figure 6 present temperature recorded by all the sensors.

Similarly, data after March 2018 (respect. 2021) are not represented for sensors B8, H9 and B10 (respect. H1 and B2) because they are too scattered to be taken into account. The violins consider all the temperatures recorded (i.e. one per hour), and not just the averages.

This preprint research paper has not been peer reviewed. Electronic copy available at: https://ssrn.com/abstract=4743392

To compare one year with another or one sensor with another we have chooses two different types of graph. Figure 5 shows classical temperature data as a function of time (each point corresponds to a weakly mean temperature) but year per year, with all plots having the same scale, while Figure 6 represents the data in form of violin plots. Each violin corresponds to one-year temperature. The larger the violin, the greater the temperature recorded over the year. The bars represent the maximum, medium and minimum values recorded. Please remember that in 2012 recording began in November, thus this is not a full-year data, which is why the violin is smaller (it only synthesises 2 months of winter). Similary, data after March 2018 (respect. 2021) are not represented for sensors B8, H9 and B10 (respect. H1 and B2) as they are too scattered to be taken into account. Violins consider all recorded temperatures (i.e. one per hour), and not just the average.

Figure 5 illustrates the classical temperature recording in an Altered Mediterranean Climate (see above the end of part 2.1). Highest temperature (weekly means between 20 and 25°C) are recorded around July (weeks 26-32) and lowest (weekly means around 0°C) around the end of January – beginning of February (weeks 1-8).

Preprint not peer reviewed

This preprint research paper has not been peer reviewed. Electronic copy available at: https://ssrn.com/abstract=4743392

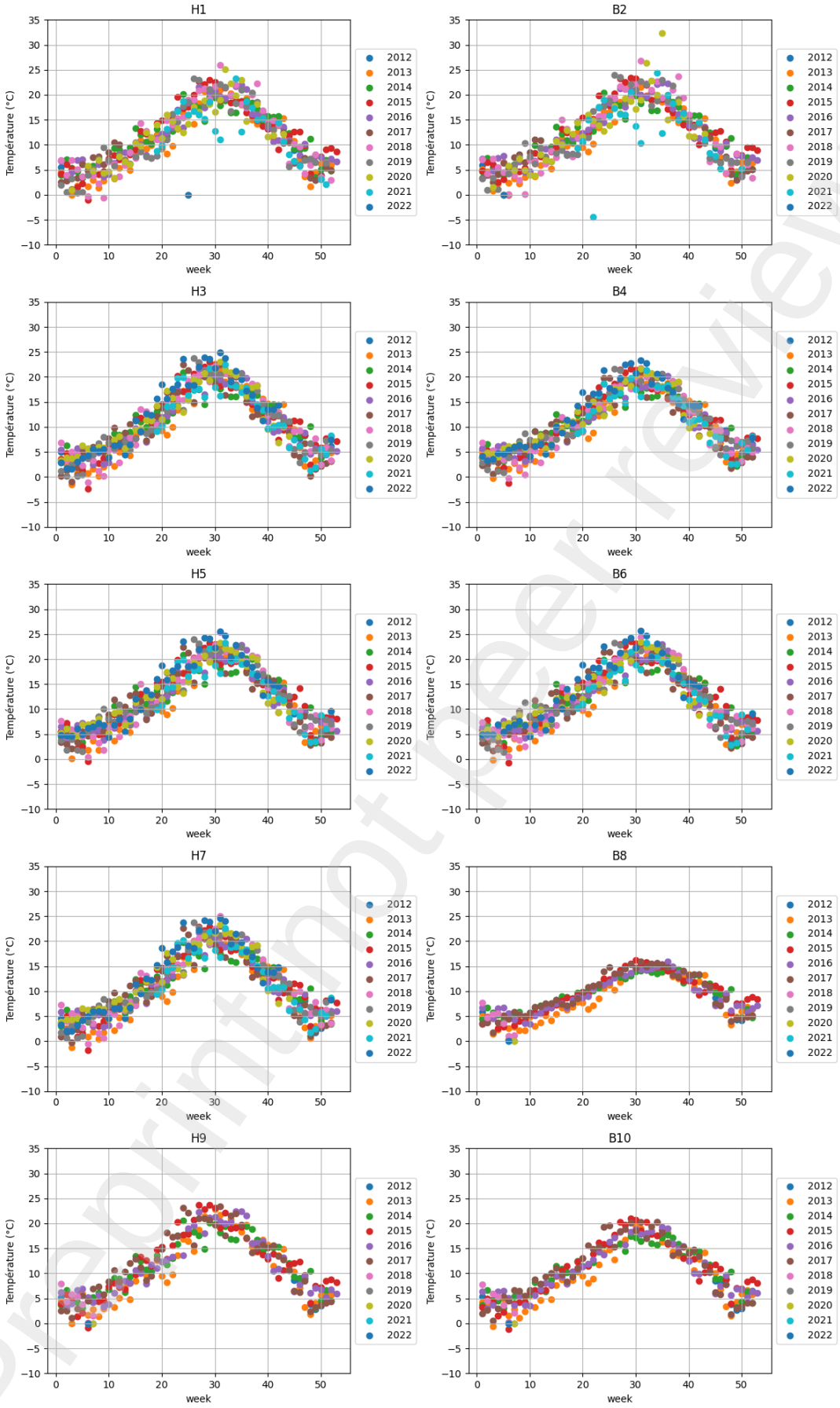

Figure 5: Weekly Mean temperature recording on sensors

Preprint not peer reviewed

This preprint research paper has not been peer reviewed. Electronic copy available at: https://ssrn.com/abstract=4743392

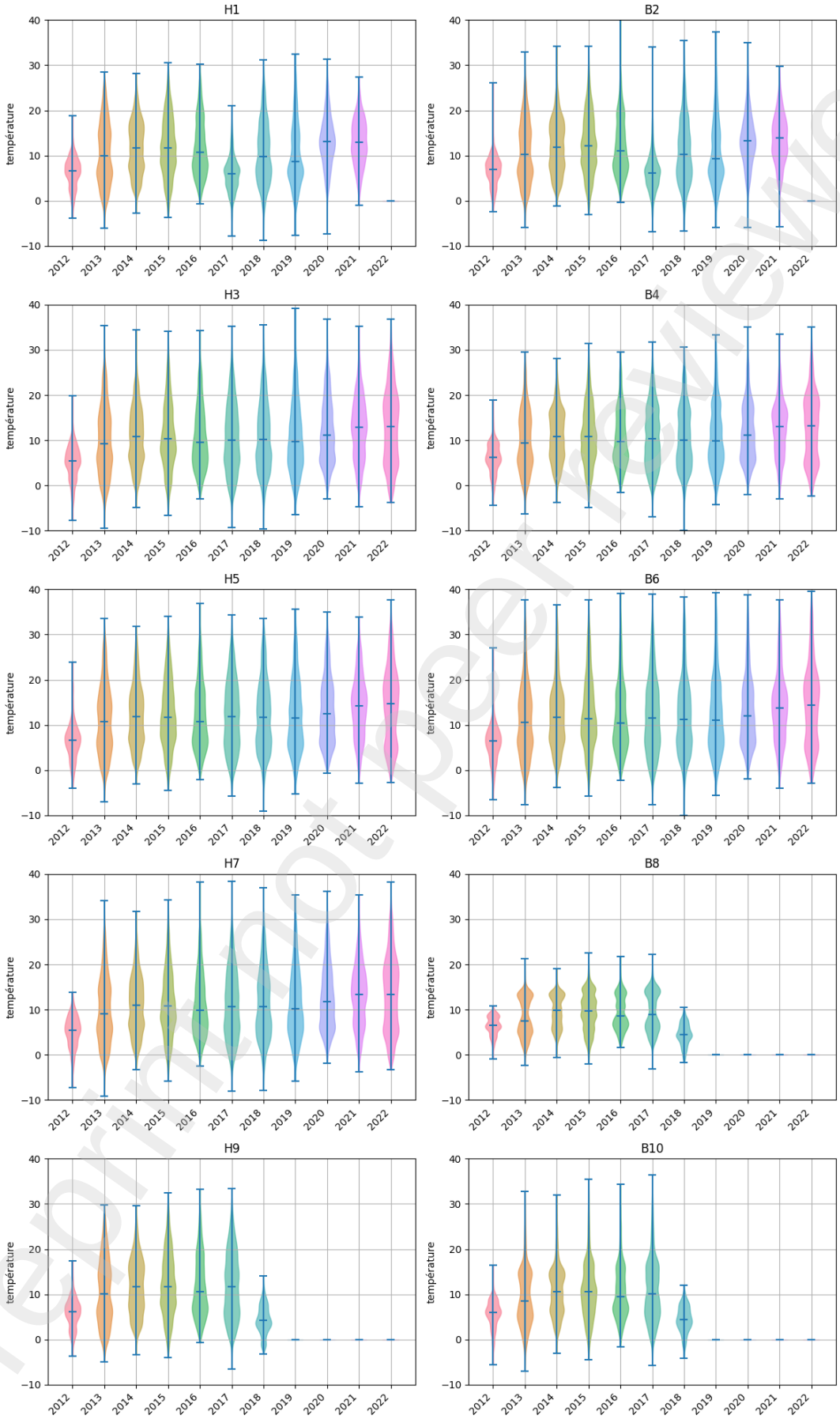

Figure 6: Temperature recording on sensors.

Preprint not peer reviewed

This preprint research paper has not been peer reviewed. Electronic copy available at: https://ssrn.com/abstract=4743392

We can observe on Figure 6 that, even if temperature variations are observed from one year to the next, there is no overall trend to be drawn from these measurements in terms of warming over the past 10 years, nevertheless a slight increase of medium values is observed in 2021 and 2022 compared to 2015-2019. When comparing high (H) and Bottom (B) sensors located on the same fracture, we observe that the yearly amplitude is larger for top sensors than from bottom. As expected, deeper in the fracture, temperatures are more regulated since they are less exposed to sunlight.

Finally, we also computed mean temperature per month as displayed in Table 2. As expected in the area, the coldest month for all sensors is January and the warmest is July for 6 sensors and August for the 4 remaining (remind that B8 and V8 have the same temperature sensor).

Table 2: Mean temperature per months

	H1	B2	H3	B4	H5	B6	H7	B8	H9	B10
January	4.09	4.72	2.93	3.81	4.59	4.65	3.32	4.05	3.75	3.62
February	4.46	5.02	3.7	4.28	5.23	5.58	4.08	4.56	4.57	4.41
March	6.74	7.2	6.09	6.2	7.47	7.6	6.28	5.76	6.73	6.28
April	9.7	10.12	9.15	8.93	10.34	10.47	9.49	8.29	9.88	9.29
May	12.04	12.36	12.48	11.46	13.01	13.03	12.64	11	12.88	12.25
June	16.73	17.07	17.51	16.01	17.6	17.45	17.5	14.75	17.76	16.63
July	19.86	20.28	20.31	18.97	20.68	20.57	20.49	17.55	20.8	19.62
August	19.4	19.93	19.47	19.05	20.73	20.93	19.89	17.68	20.37	19.48
September	16.83	17.35	15.48	16.19	17.55	17.65	16.14	15.27	16.69	16.17
October	12.81	13.11	11.37	12.1	13.22	13.1	11.9	11.77	12.42	12.02
November	8.37	8.79	6.61	7.42	8.3	8.07	7.06	7.81	7.61	7.39
December	5.95	6.31	4.5	5.21	6.09	5.91	4.81	5.69	5.31	5.22

3.1.2 Daily temperature amplitude

All daily temperature amplitudes were calculated. Maximum daily amplitude recorded on each device is given in Table 1. To be more readable, week means daily amplitudes are displayed in Figure 7 per year as a function of the considered week and Figure 8 shows the mean temperature as a function of the daily amplitude, values averaged over a week. Colours are kept the same on all plots to be able to compare data from one year to another.

Considering both figures together we can say that, overall, when daily mean temperatures increase, daily amplitude increase. It has been verified by statistical analysis of the data (correlation, significance and variance analysis) not presented here. This trend is a general trend, represented in Figure 7 by bell-shaped curves and in Figure 8 by a global linear positive trend, easier to see on H3, H7, B10 sensors. Beyond this general trend, some more local behaviour can also be observed:

- Very high daily amplitudes can occur even when the mean daily temperature is low (winter periods). It probably occurs on sunny days, even if it cannot be proved with our monitoring device.
- Even more, there is more variability in thermal amplitudes when the average temperature is low than when it is high: daily amplitude values evolve more from one week to another during winter months than summers. It can be easily observed in Figure 8 on sensor H5 and B6 with cone-shaped curves, for instance.

Preprint not peer reviewed

This preprint research paper has not been peer reviewed. Electronic copy available at: https://ssrn.com/abstract=4743392

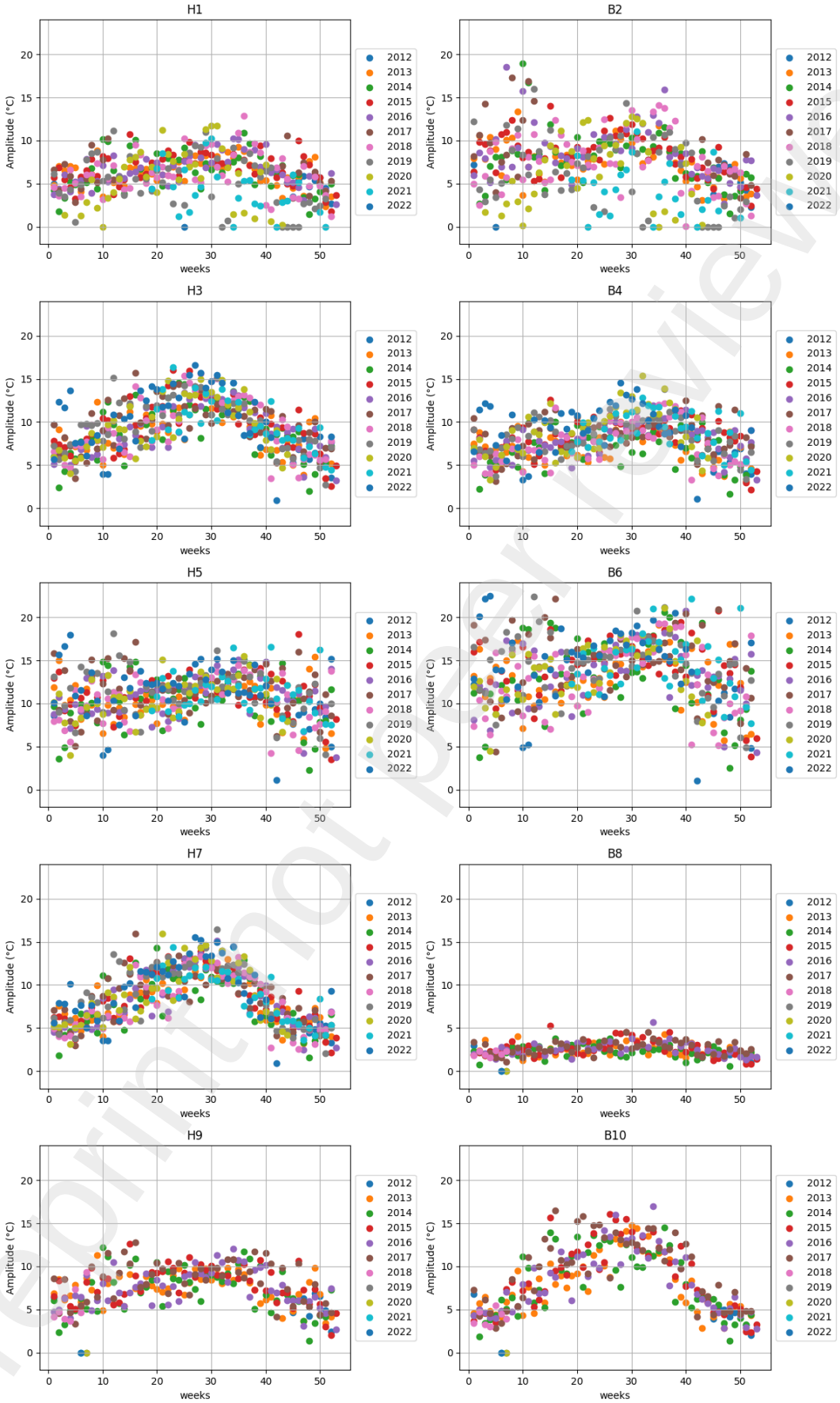

Figure 7: Distribution of daily amplitudes as a function of temperature - weekly means – scale and colours are kept the same for all plots.

This preprint research paper has not been peer reviewed. Electronic copy available at: https://ssrn.com/abstract=4743392

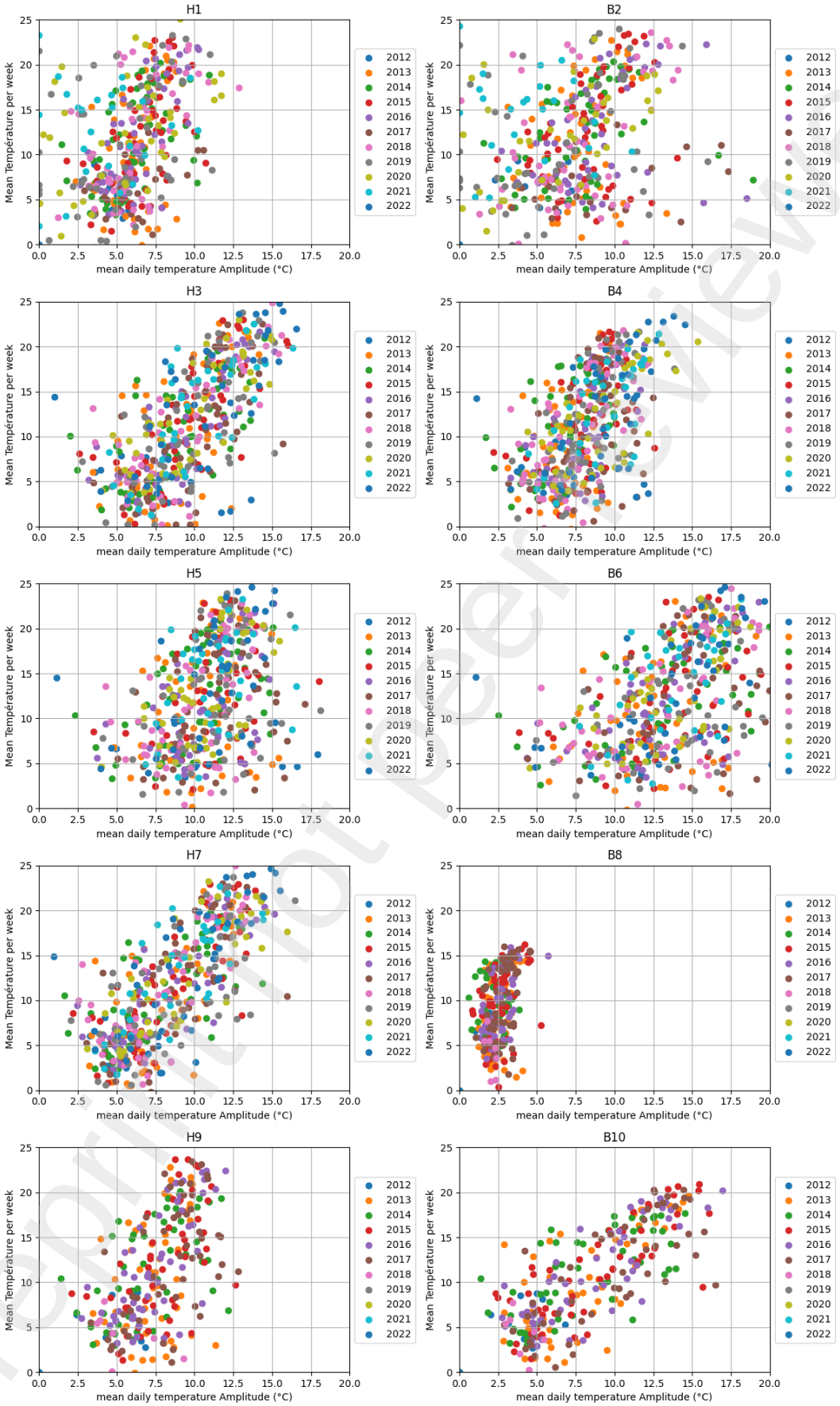

Figure 8: Distribution of weekly mean temperature as a function of daily temperature amplitude (one week average) – scale and colours are kept the same for all plots.

This preprint research paper has not been peer reviewed. Electronic copy available at: https://ssrn.com/abstract=4743392

3.1.3 *Comparison of the kinetics of temperature variations*

Figure 9 shows two consecutive days for each season. The temperature data are not smoothed, and one measure per hour is displayed. The days are chosen at random to be as representative as possible, although periods with missing data were not considered. As expected, given the local climate, temperature amplitudes are greater in winter (when the sun shines) and in summer than in spring or autumn. We decided here to focus on 2 consecutive days to compare temperature trends. With such representation, it is difficult to propose general conclusions because no systematic behaviour is observed. For instance, on the 4th of January 2013 (Figure 9a) the temperature of sensors B4, H5, B6 increase more quickly than the temperature of sensors B2 and H3 whereas the following day B2, H3, B4 increase before H5 and B6.

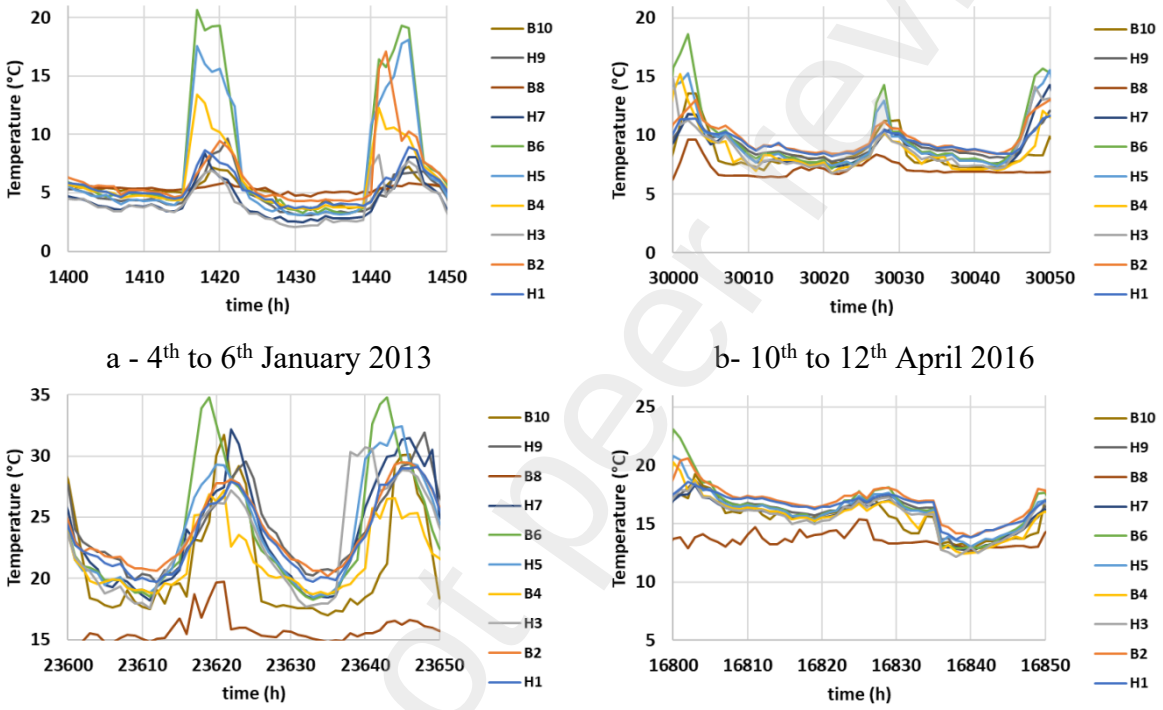

a - 4th to 6th January 2013

b- 10th to 12th April 2016

c- 18th to 20th July 2015

d- 8th to 10th October 2015

Figure 9: Temperature recordings – zoom in 2 days per season. Scale is the same for all figures

The evolution rates will be discussed deeper in the discussion part (4.3).

3.2 *Displacement recording*

All displacement curves are given in appendix 3. As done for temperature (Figure 4 and appendix 2), to make the curves more readable, daily means and weekly means were computed, and the data after February 2018 for B8, H9 and B10 and after 2021 for H1 and B2 are not displayed as the records have too much noise. Displacements curves are presented 2 by 2 on the same graph (H and B for the same global location). Weekly mean displacements are represented by dots and weekly maximum and minimum are represented by an error bar.

3.2.1 *Global analysis*

Analysis of the curves show different results depending on the location of the sensors, but some general trends can be observed (see displacement curves presented on appendix 3):

Preprint not peer reviewed

This preprint research paper has not been peer reviewed. Electronic copy available at: https://ssrn.com/abstract=4743392

- annual cycles can easily be seen on the displacement curves (as for temperature curves),
- displacement curves seem to evolve more erratically than temperature curves,
- unlike the temperature curves which remain generally constant from one year to the next, the deformation curves show a drift with time,
- the drift can be positive or negative depending on the sensor under consideration,
- H and B sensors of the same location evolve in the same way: their drift has the same symbol (H1, B2, H3, B4 present negative drift and H5, B6, H9, B10 have positive drift). A negative drift means that rock faces tend to get closer to each other, a positive one means that both rock faces tend to separate from each other. This will be discussed later.

Comparing H and B sensors of the same location, we can add:

- Daily and weekly displacement amplitude is larger on B-sensors than on corresponding H-sensors except for H9 - B10. This is illustrated by the length of the bars in Annexe 3 figures.
- A larger drift is observed on H-sensors displacement than on B-sensors when the drift is negative and a smaller when the drift is positive, if we focus only on the first 6 sensors (H1 to B6) as H7 to B10 are more difficult to analyse 2 by 2.

3.2.2 Comparison of sensors placed at the same high but at the front or rear

Figure 10 compare displacements curves obtained at approximately the same height but at the front (H5, B6) or rear (H3, B4). The upper part of Figure 10 focuses on the H sensors (H5, dots in red, error bar in blue and H3, dots in green, error bar in yellow) and the lower part on B sensors (B6, dots in red, error bar in blue and B4, dots in green, error bar in yellow).

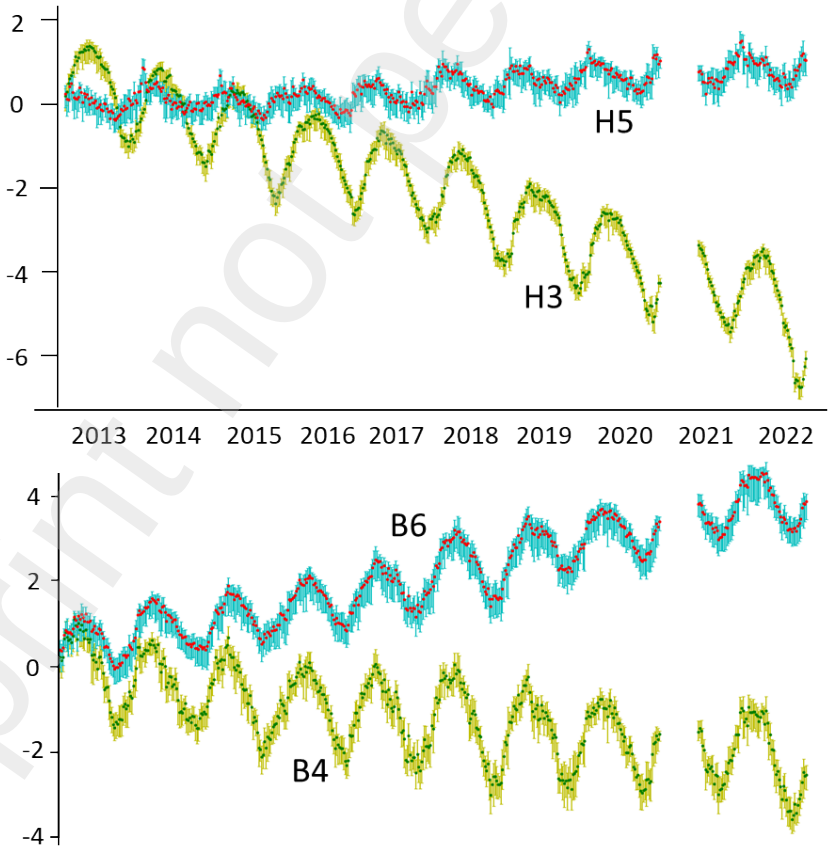

Figure 10. Comparison front face H5 and B6 (dots in red, error bar in blue) / backward face H3 and B4 (dots in green, error bar in yellow)

Preprint not peer reviewed

This preprint research paper has not been peer reviewed. Electronic copy available at: https://ssrn.com/abstract=4743392

We can see that displacements are evolving simultaneously: on a yearly scale, a displacement peak on one sensor is mirrored on the others. In terms of weekly variations in displacement amplitude, H5 and B6 appear to be more dispersed than H3 and B4. On the other hand, if we look at annual displacement amplitudes, H5 and B6 are smaller than H3 and B4. Finally, regarding trends (drifts), sensors located at the same level show trends of opposite sign (displacements on H5 overall increase, while those on H3 tend to decrease; similarly, displacements on B6 increase, while those on B4 tend to decrease.

3.2.3 Oder of magnitude

Figure 11 presents the comparison between horizontal and vertical displacement corresponding respectively to B8 and V8 sensors between 2012 and 2018. We can observe that a slope of -0.8 can fit the curve from part to part. This observation will be discussed in the mechanical analysis part.

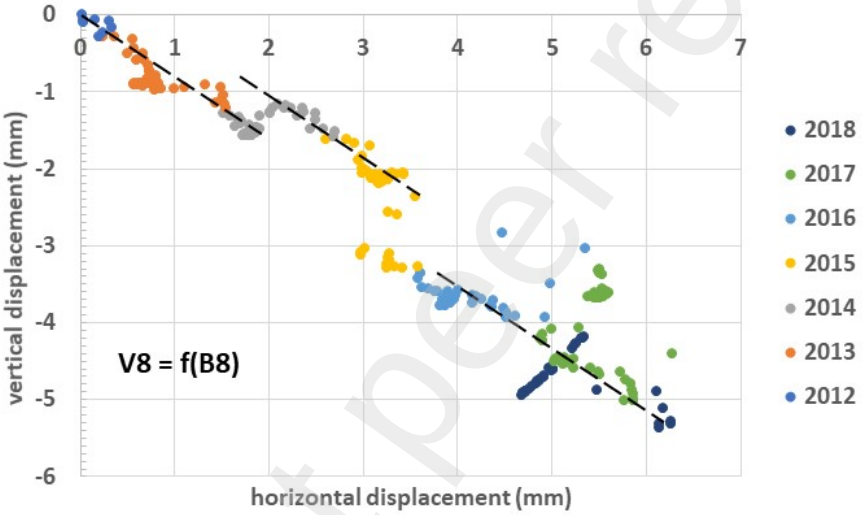

Figure 11 : Comparison of horizontal (B8) and vertical displacements (V8)

3.3 Displacement versus temperature curves

3.3.1 Daily / weekly comparison

Figure 12 presents displacements and temperature recorded on sensor B4. Displacement peaks correspond broadly to temperature peaks (see on Figure 12a), but in detail it is not quite as simple. In fact, the curve displacement = f(temperature) on Figure 12b is not a straight line even if the tendency is a linear behaviour. Overall, an increase (respectively decrease) in temperature leads to an increase (respectively decrease) in displacement. In most cases, this variation is concomitant. But, looking deeper in the data show that the same increase (or decrease) of temperature does not imply the same displacement variation depending on the mean temperature. For low temperatures, the temperature increment required to obtain a displacement increment is relatively small (1 or 2 degrees). If the temperature is higher, the same increment of 1 or 2 degrees will not lead to an increment in displacements - it may need 3 or 4°C to have one. This shows that the system is not purely elastic.

On a weekly scale, a moving 4-hour average is sufficient to smooth out some of the local variations, but on a monthly or yearly scale we need to enlarge the moving average to smooth the curves. Instead of a few days moving average, we choose to calculate weekly means and plot them together with weekly min and weekly max temperature (see curves on appendix A2).

Preprint not peer reviewed

This preprint research paper has not been peer reviewed. Electronic copy available at: https://ssrn.com/abstract=4743392

Displacements are function of the temperature variations, the direction of variation (increase or decrease) and the average temperature over a week.

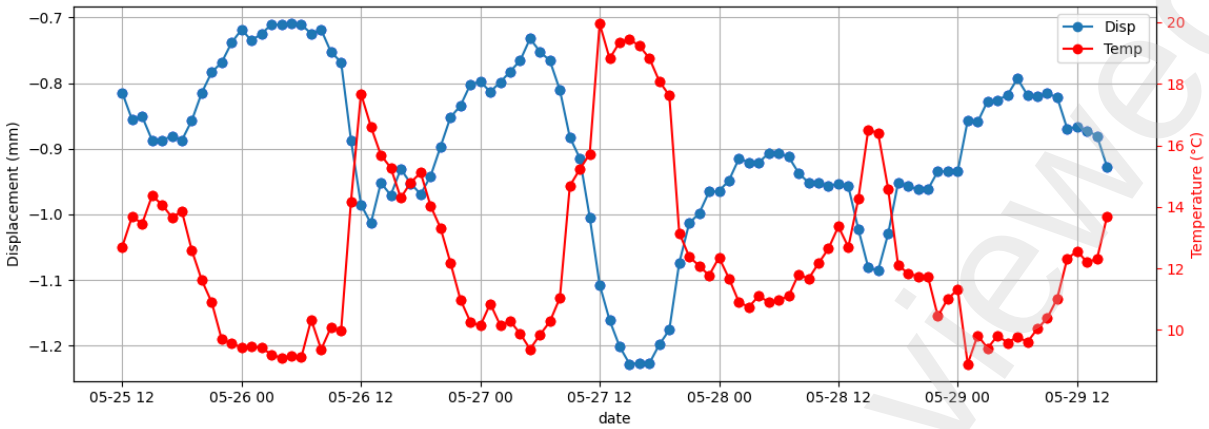

a

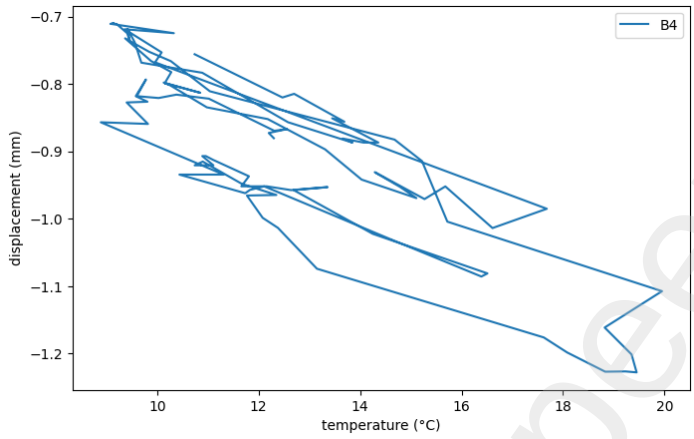

b

Figure 12 : Displacement and temperature recorded on B4 sensor between 2016/05/25 and 2016/05/29. a- as a function of time, b- displ = f(temp)

3.3.2 Evolution over 6 years

Figure 13 presents recorded displacements versus recorded temperature in H3, B4, H5 and B6 all sensors. On Figure 13 smoothed curves plotted with monthly averages are shown over the 10 years recorded. The cyclic behaviour is obvious. Appendix 4 presents all curves for the period 2012-2018, presented with weekly averages (dots are not linked to help to be more readable). Scales are kept the same for each H/B pairs, except for H5/B6 and H7/B8, and each colour corresponds to a year and year colours are the same for all sensors. On Figure 13 and in Appendix 4 black arrows correspond to an annual hysteresis, red line is the annual displacement range between min and max temperature and blue arrows correspond to a 10-years drift on Figure 13 and a 6 years-drift in appendix 4. Parameters measured on appendix 4 curves are given in Table 3 (6 years drift) and parameters measured on *Figure 13* curves are given in Table 4.

The vertical translation of the curves "displacement vs temperature", means that displacements evolve even if the annual temperature range does not. This is a strong indication of the cumulative effect of the temperatures on displacements.

Preprint not peer reviewed

This preprint research paper has not been peer reviewed. Electronic copy available at: https://ssrn.com/abstract=4743392

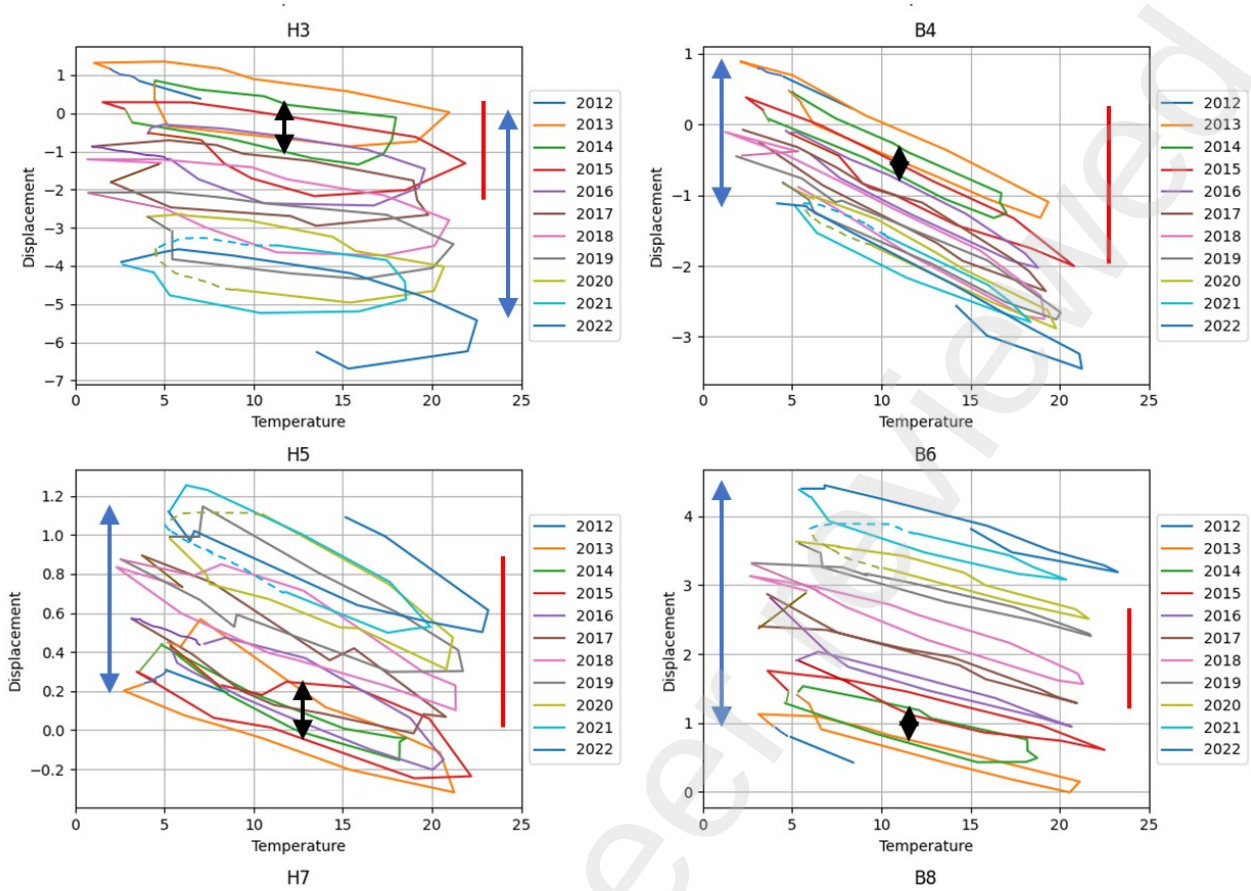

Figure 13. Displacement versus temperature on High (left) and Bottom (right) sensors. Each dot corresponds to a week mean value. Colors are identical on all graph, but displacements scales are not the same. Blue arrows correspond to a 10-years drift, black arrows correspond to an annual hysteresis. Red line is the annual displacement range between min and max temperature.

Table 3: Measured parameters obtained on the curves presented in appendix 4 (2012-2018) – estimation of the parameter are based on weekly means.

	Annual displacements range (mm)	annual hysteresis (mm)	6-year drift (mm)	Comments
Appendix 4	*Red line*	*black arrow*	*blue arrow*	
H1	- 2.25*	0.3	-1.4	*smaller in 2015 2017: Only partial data
B2	- 2	0.3 to 0.4	- 0.8 to -1	4-years drift Data after 2016 are not considered
H3	-2.5	2	-2.5 to 3	
B4	-2.5	0.5	-1.1 to -1.5	
H5	0.95	0.5	0.5 to 0.6	
B6	1.7	0.3	2	
H7	-0.5	0.35	-0.9 to -0.95	
B8	1.1	1.1	4 to 5.5	
V8	1.6	1.2	4 to 4.6	
H9	2.1	1.3	1.5	
B10	2.5	1.55	1.3 to 1.5	

Preprint not peer reviewed

This preprint research paper has not been peer reviewed. Electronic copy available at: https://ssrn.com/abstract=4743392

Table 4: Measured parameters obtained on the curves presented in Figure 13 (2012-2022) - estimation of the parameter are based on monthly means.

	Annual displacements range (mm)	annual hysteresis (mm)	10-year drift (mm)
Figure 13	*Red line*	*black arrow*	*blue arrow*
H3	- 2.6	1.3	- 5.5
B4	- 0.9	0.4	- 2
H5	2.15	0.3	1
B6	1.5	0.5	3.6

H3 and B4 behaviour have been already described in (Gasc-Barbier et al., 2023) only for the first 6 years of recording. After 10 years of recording, the total effect is a decrease in displacement of about 2 mm on B4 and of about 5.5 mm on H3, as illustrated with the blue arrows on *Figure 13* and values given on Table 4. They are consistent with values given on Table 3 and (Gasc-Barbier et al., 2023) for a 6-year drift. In addition, there is a difference between the measured hysteresis of each annual *Dp vs T* curves. On the one hand, on both sensors the hysteresis is almost constant from year to year, but, on the other hand, the annual hysteresis (see black arrows) is nearly 3 to 4 times smaller on B4 (about 0.4, 0.5 mm) than on H3 (about 1.3 to 2 mm) depending on the representation by weekly means or monthly means. The choice of the way to represent data is emphasised by the annual displacement range (red lines): values obtained on 6 years curves and weakly means as presented in appendix 4 show that the amplitude of displacements between max and min temperatures is the same on both sensors, whereas 10 years curves and monthly means as presented in *Figure 13* does not show the same trend.

4 DISCUSSION

4.1 Displacements' seasonality

Figure 14 presents a synthesis of the evolution of displacement during the year. Each dot corresponds one average weekly displacement, and graphs are plotted with a colour per year, to show the potential evolution. Most of the curves have a v-shape and present a minimum between week 20 (mid-May) and week 40 (end of September) and a maximum between week 45 (early November) to week 10 (mid-March). To be more precise: B2 (except 2021), H3, B4 (except 2021 and 2022) and H7 have their minimum in September (weeks 36-39), B1, B4, B6, H9 in August (weeks 31-34) and only H5 has its minimum at the end of July – beginning of August (weeks 29-32). On the opposite, maximum is obtained in December for H5, in January (weeks 1-4) for H1, B2, B4, H7, and in February for B6, H9. H3 has its maximum in early March (week 10).

If we compare these results with temperature recordings (see Figure 5), we can observe that maximum and minimum are not perfectly correlate. There is a slight time lag between peaks. This effect is particularly noticeable on H3, B4 and H9. Maximum temperature is respectively obtained weeks 29-31, 29-31 and 27-30 whereas minimum displacement is obtained weeks 35-38, 30-33 and 33-36. This slight time lag of 2 to 4 weeks is not as easily observed during winter months and seems to be reduced to only 1 or 2 weeks which is more difficult to see.

Preprint not peer reviewed

This preprint research paper has not been peer reviewed. Electronic copy available at: https://ssrn.com/abstract=4743392

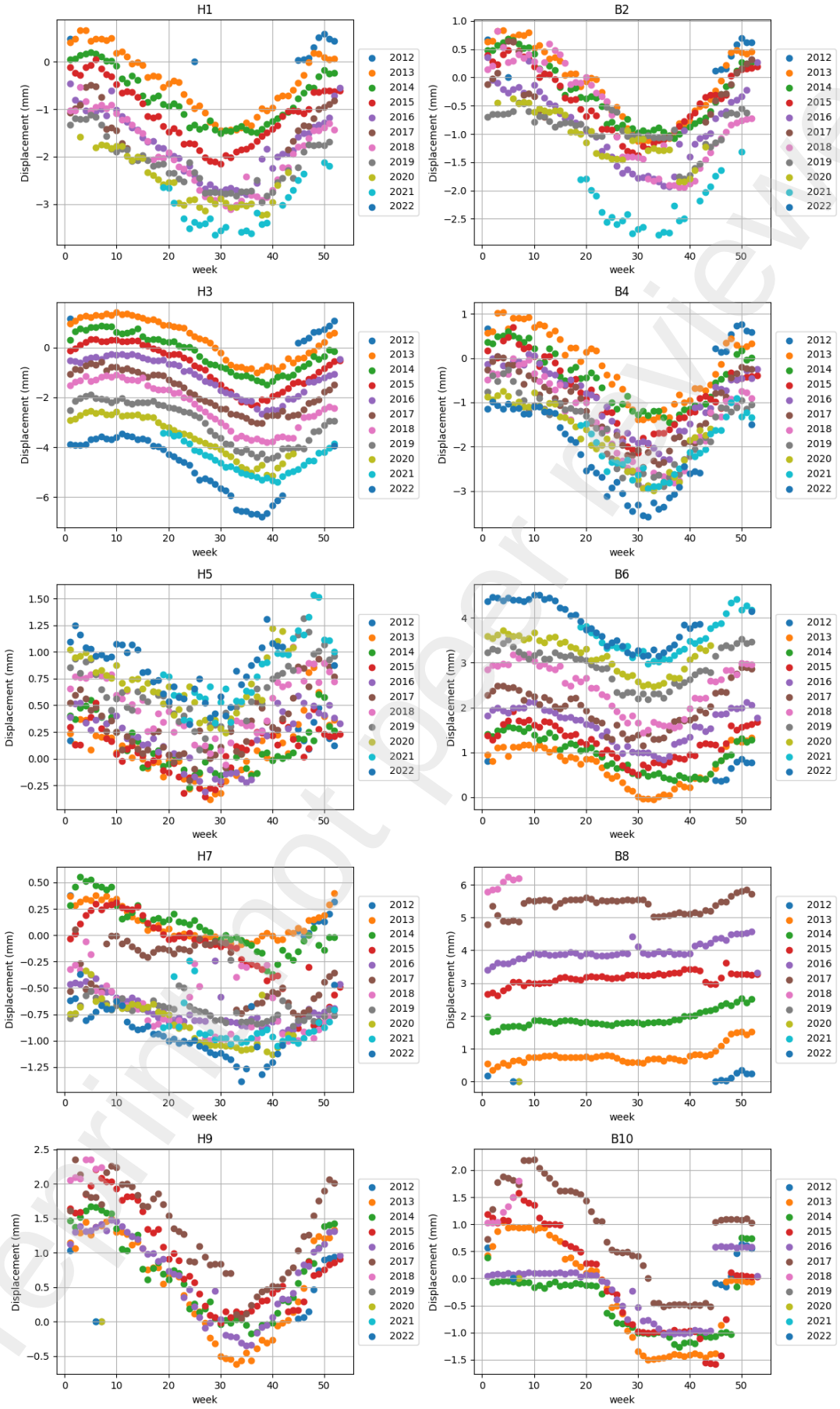

402
403

Figure 14 : Average weekly displacements mean during the year

Preprint not peer reviewed

This preprint research paper has not been peer reviewed. Electronic copy available at: https://ssrn.com/abstract=4743392

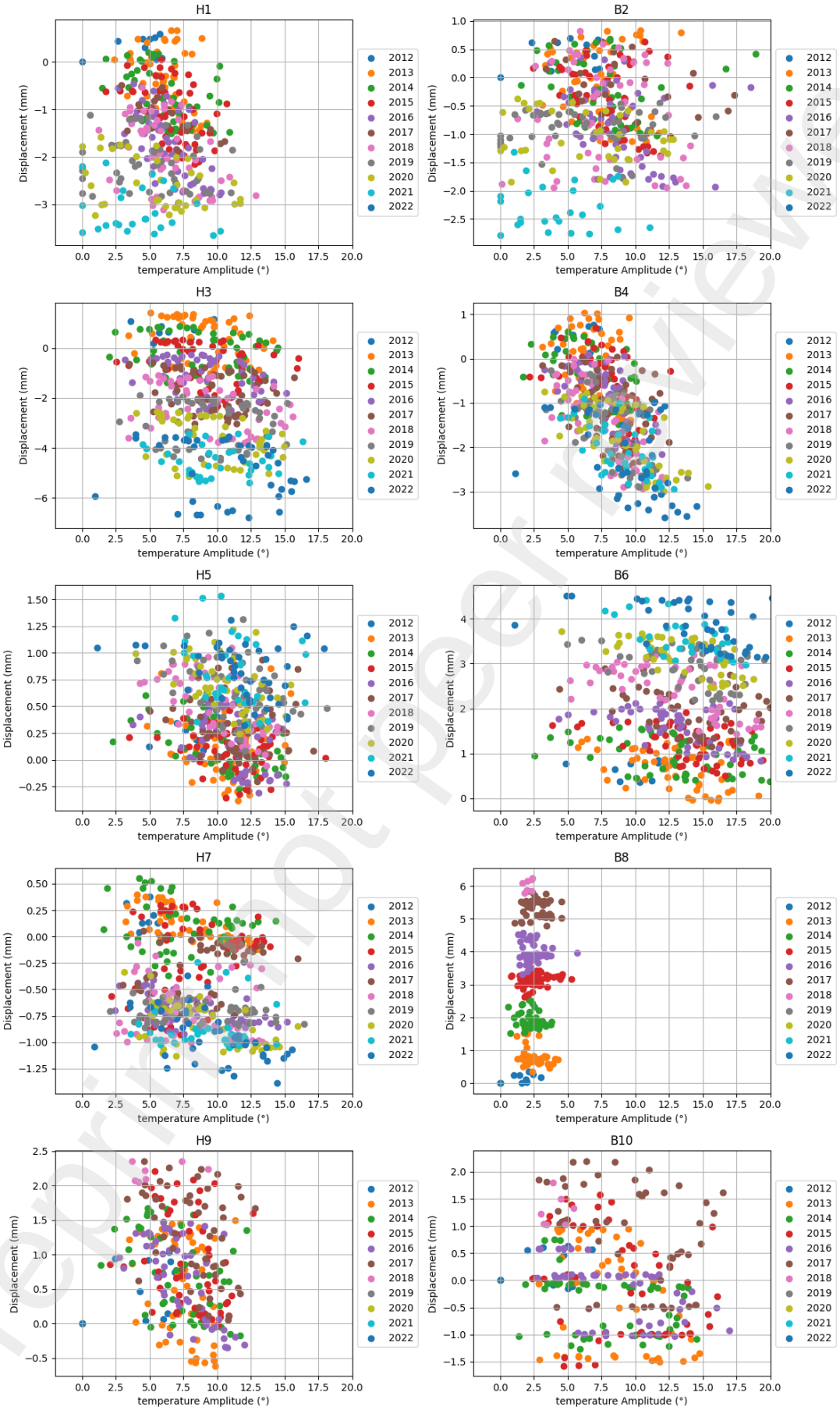

404
405

Figure 15 : displacements as a function of the daily amplitude of temperature

Preprint not peer reviewed

This preprint research paper has not been peer reviewed. Electronic copy available at: https://ssrn.com/abstract=4743392

4.2 *Displacements as a function of the daily amplitude of temperature*

Figure 15 presents recorded displacements as a function of the daily amplitude of temperatures averaged over a week. The colours of the years are the same as those of the previous plots. In contrast to the results shown in Figure 14, it is very difficult to find a trend on Figure 15. The curves seem to have no characteristic shape. In the same way, if we compare Figure 15 with *Figure 13* or appendix 4 (displacements versus temperature) no global analysis can be proposed. Thus, it is another clue to say that the value of the daily amplitude does not play a significant role on displacements whereas the repetition of cycles does.

4.3 *Influence of temperature increment on displacement increment*

As mentioned earlier, the link between variation of temperature and evolution of displacement is established (see 3.3 and figure 11), but the evolution is more complex than just a simple proportional relation, which would have corresponded to a thermoelastic behaviour between increment of temperature and increment of displacement. To look deeper how temperature modifies displacement and, considering the previous observations (section 3.3), here we focus on their incremental evolution and performed multiple linear regression. To avoid bias as far as possible we decided to focus only on H3, H5, B4 and B6 which seems to be the more reliable sensors. On those 4 sensors, data sorting was realised:

1. Incremental displacement (Δd_i) and incremental temperature (ΔT_i) were calculated only if successive measurement were one hour apart.
2. Δd_i are kept for multiple linear regression analysis only if ΔT_i, ΔT_{i-1}, ΔT_{i-2} and ΔT_{i-3} are available.

When using B6 as an example of data processing, from about 87600 measurements (which correspond to a measure each hour for 10 years), only 76791 were used for all former analysis (due to lack in measurements or not reliable values) and then 66452 were kept for multiple linear analysis. Even if the exact number is not the same on all sensors, the proportion is similar. Histograms of incremental values were prepared to verify the homogeneity and the repartition of the measurements. All shows a Gaussian repartition which tends to show that no "erroneous" values were kept.

Simple 2- by- 2 correlation between incremental displacements and incremental temperatures were realised and the calculates correlation coefficients are presented on Table 5. For all sensors, the best correlation is obtained with the corresponding temperature increment, but it can be seen that previous increments also have a significant weight. It also appears that on B sensors, the 2-hours previous increment (ΔT_{i-2}) plays a more important role (it has a higher correlation coefficient) than the 1-hour previous increment (ΔT_{i-1}). This is not the case with H sensors, where the order of importance follows the expected order (the further before, the less significant).

Table 5: Correlation coefficients between incremental displacement and incremental temperature

R^2	$\Delta d_i=f(\Delta T_i)$	$\Delta d_i=f(\Delta T_{i-1})$	$\Delta d_i=f(\Delta T_{i-2})$	$\Delta d_i=f(\Delta T_{i-3})$
B4	0.3671	0.0963	0.1874	0.057
B6	0.3014	0.1688	0.206	0.1816
H3	0.1336	0.0614	0.0149	0.006
H5	0.6521	0.2572	0.1616	0.0979

Preprint not peer reviewed

This preprint research paper has not been peer reviewed. Electronic copy available at: https://ssrn.com/abstract=4743392

Multiple linear regression analysis was then performed on the four sensors data. It consists in finding the coefficients a, b, c, d, e that give the best fit to the equation written as:

$$\Delta d_i = a * \Delta T_i, + b * \Delta T_{i-1}, + c * \Delta T_{i-2} + d * \Delta T_{i-3} + e$$

The values of the best-fitted coefficients and the correlation coefficients of the multiple linear regression are given in Table 6. Values are given with 6 digits for a better comparison. As expected, correlation coefficients of the multiple linear regression analysis are higher than those presented on Table 5 which emphasise the importance of not only the concomitant temperature increment but also the formers.

Table 6: Results of the multiple linear regression analysis

	a	b	c	d	e	R^2
B4	0.014762	0.005392	0.010608	0.004118	-0.000937	0.5505
B6	0.009976	0.003625	0.005440	0.006379	-0.001695	0.508
H3	0.007247	0.003080	0.001372	0.000115	-0.000331	0.1607
H5	0.015766	0.005630	0.003675	0.003035	-0.000577	0.7881

4.4 Proposition of a mechanical interpretation

4.4.1 From a local point of view

The previous observations on the influence of past temperature increments on the current displacement increment can be translated from a mechanical point of view with the rheological spring-sliding element. Further investigations are needed to be able to formalise properly such constitutive law, but our observations seem to show that to reproduce the thermomechanical coupling, thermoelasticity is no sufficient. Viscoplasticity with dashpot should at least be considered to reproduce the observed drift during years and, moreover, sliding element should also be used to better reproduce the in-situ observations.

Comparison of displacement recorded on B8 and V8 sensors give a -0.8 slope (see Figure 11). If the behaviour was isotropic, we should have a 1 slope. The difference between 0.8 and 1 correspond to an angle of about 6° that be attributed to a local rotation of the rock mass, and more precisely considering the location of the sensors, between B_1 and B_2.

4.4.2 From a global point of view

Results presented above enable us to the propose schematic evolution of the shape of column B with temperature displayed in Figure 16, in the short term: when temperature decrease rock mass globally shrinks, the rock faces move away from one another and displacements recorded on sensor (displayed between rock faces) are positive (Figure 16b). When temperature increase, the volume of the rock mass globally increases, the rock faces are getting closer and displacements recorded on sensor (displayed between rock faces) are negative (Figure 16c). This can be considered as the normal “breathing’ of the rock mass, that is an elastic evolution in thermoelasticity.

Preprint not peer reviewed

This preprint research paper has not been peer reviewed. Electronic copy available at: https://ssrn.com/abstract=4743392

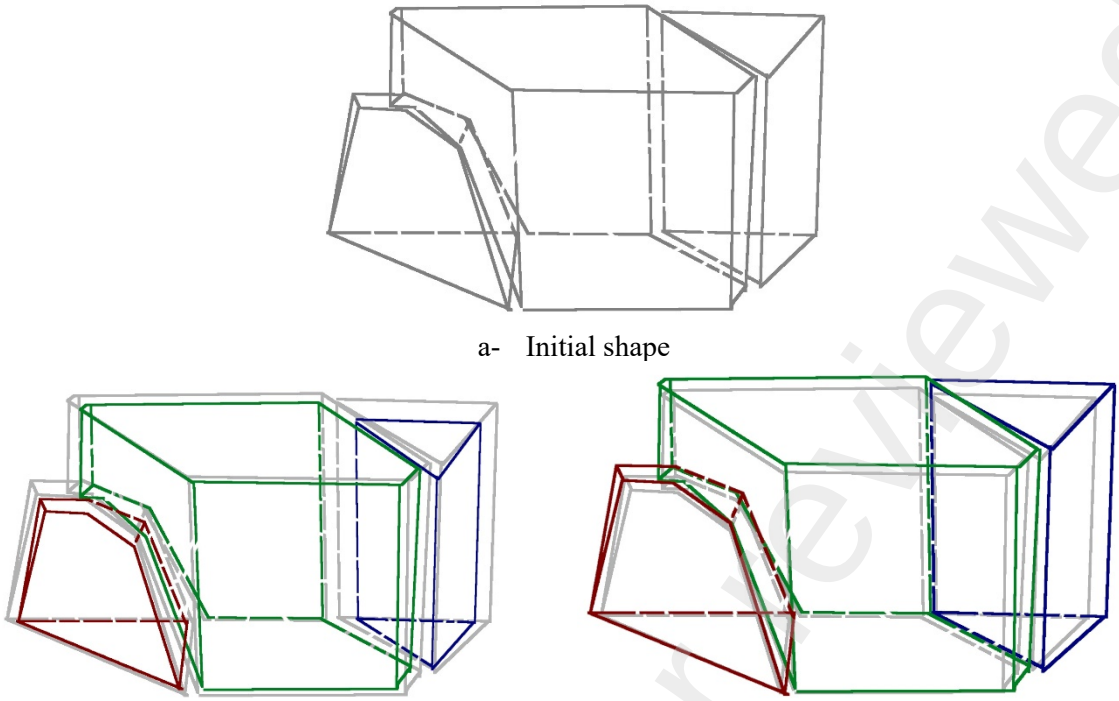

a- Initial shape

b- After temperature decrease

c- After temperature increase

Figure 16 : schematic evolution of the shape of column B with temperature. In grey: initial shape, in red sub-column B1, in green: B2, in blue: B3

In the longer term, when considering the general evolution of displacements with temperature, during the 10 years, between 2013 and 2022, we can measure a mean displacement drift twice smaller on B4 than on H3. Considering the general movement of a column, which is an oscillation, it is not surprising to observe that the movement of the top of the column is greater than the movement of the base. What is more surprising is the global relative movement of the column: a negative drift in displacement means that the column tends to move closer to the rock wall, which is surprising. As mentioned earlier, the top of the column is farther from the cliff than the bottom. Some assumption can be proposed:

- joint opening: if joints opened in the column itself or in the rock mass, it could lead to bring opposite walls closer, a fracture exists on site (see B6 sensor) but this analysis need to be investigated deeper to validate this assumption.
- iA rotation of the column, if its gravity centre is towards the rear. Even if an estimate of the position iof the gravity centre was propose in § ?? the geometry of the column is not precise enough (no laser scan for instance is available) to support this hypothesis
- B column could also punch the infra-bathonian interlayer limestone but no topographic measurement was displayed in 2012 to validate or not this assumption.
- lateral interaction between the column and other rock masses that could limit and constrain the movement of the column can also be evoked.

4.5 Comparison of observations with other sites

The observations and measurements realised on *les chandelles de l'Escalette*, are consistent with those obtained on other sites. As mention formerly, (Merrien-Soukatchoff and Gasc-Barbier, 2023) proposed a synthesis on the effects of natural thermal cycles on rock outcrops and pointed out different studies. Most of the displacement's measurements realised along

This preprint research paper has not been peer reviewed. Electronic copy available at: https://ssrn.com/abstract=4743392

fractures (Bakun-Mazor et al., 2020, 2013; Cloutier et al., 2015; Gischig et al., 2010; Grøneng et al., 2011; Marmoni et al., 2020) show the same type of drift, but the range of the evolution depends on the properties of the rocks under study. When comparing data only obtained under positive temperature (Bakun-Mazor et al., 2013) measured in Massada (Israel) about 0.35 mm of displacement amplitude (measurements last 25 months under 20 to 50°C) whereas (Guerin et al., 2021) measured on granite exfoliation sheets, a 6 mm displacement amplitude (measurements last 24 hours under 16 to 37°C) and (Virely et al., 2021) measured on a limestone cliff a 1 mm displacement variation (measurements last 4 years under 5 to 35°C).

5 CONCLUSION

From an operational engineering point of view, the 10 years of recording have enabled us to understand the overall functioning of the *chandelles de l'Escalette* as proposed in figure 16, and to rule out the rock hazard for the road, even if questions remain concerning the very long-term evolution of the massif.

From an understanding point of view, thanks to its sensors distributed in different positions, and, above all, thanks to the duration of the measurements, the analysis of this site was able to show the complex link between natural thermal variations and mechanical variations. If, in the short term, looking at data over a few weeks for example, we observe a globally proportional relationship between displacements and temperature, we can clearly see that when longer recordings are available, this simple thermoelasticity hypothesis no longer works. To take account of this drift, it is then necessary to propose mechanical models with damage, i.e. to choose between viscoplastic or thermal fatigue behaviour laws.

Finally, an important contribution of this work is the identification of the inertia of the system. Indeed, it seems that a given temperature increment will not lead to the same displacement increment. The immediately preceding temperature history also plays a role in the recorded displacement increment. This study is therefore a further step towards proposing a phenomenological behaviour law to describe thermomechanical coupling in fractured massifs subjected to natural temperature variations.

Supplementary material

Data are available on request. Please contact the authors

References

Alcaíno-Olivares, R., Ziegler, M., Bickel, S., Leith, K., Perras, M.A., 2023. Monitoring and Modelling the Thermally Assisted Deformation of a Rock Column Above Tomb KV42 in the Valley of the Kings, Egypt. Rock Mech. Rock Eng. 56, 8255–8288. https://doi.org/10.1007/s00603-023-03458-1

Bakun-Mazor, D., Hatzor, Y.H., Glaser, S.D., Carlos Santamarina, J., 2013. Thermally vs. seismically induced block displacements in Masada rock slopes. Int. J. Rock Mech. Min. Sci. 61, 196–211. https://doi.org/10.1016/j.ijrmms.2013.03.005

Bakun-Mazor, D., Keissar, Y., Feldheim, A., Detournay, C., Hatzor, Y.H., 2020. Thermally-Induced Wedging–Ratcheting Failure Mechanism in Rock Slopes. Rock Mech. Rock Eng. 53, 2521–2538. https://doi.org/10.1007/s00603-020-02075-6

Preprint not peer reviewed

This preprint research paper has not been peer reviewed. Electronic copy available at: https://ssrn.com/abstract=4743392

Balducci, V., 2007. Rainfall thresholds for the initiation of landslides. Meteorol. Atmospheric Phys. 239–267. https://doi.org/10.1007/s00703-007-0262-7

Bernardie, S., Desramaut, N., Malet, J.-P., Maxime, G., Grandjean, G., 2014. Prediction of changes in landslide rates induced by rainfall. Landslides 12. https://doi.org/10.1007/s10346-014-0495-8

Bezak, N., Mikoš, M., 2021. Changes in the rainfall event characteristics above the empirical global rainfall thresholds for landslide initiation at the pan-European level. Landslides 18, 1859–1873. https://doi.org/10.1007/s10346-020-01579-0

Bièvre, G., Franz, M., Larose, E., Carrière, S., Jongmans, D., Jaboyedoff, M., 2018. Influence of environmental parameters on the seismic velocity changes in a clayey mudflow (Pont-Bourquin Landslide, Switzerland). Eng. Geol. 245, 248–257. https://doi.org/10.1016/j.enggeo.2018.08.013

Breytenbach, I.J., 2022. Seasonal bedrock temperature oscillations and inversions as a function of depth and the implications for thermal fatigue. Phys. Geogr. 43, 401–418. https://doi.org/10.1080/02723646.2020.1847242

Chigira, M., 2009. September 2005 rain-induced catastrophic rockslides on slopes affected by deep-seated gravitational deformations, Kyushu, southern Japan. Eng. Geol. 108, 1–15. https://doi.org/10.1016/j.enggeo.2009.03.005

Cloutier, C., Locat, J., Charbonneau, F., Couture, R., 2015. Understanding the kinematic behavior of the active Gascons rockslide from in-situ and satellite monitoring data. Eng. Geol. 195, 1–15. https://doi.org/10.1016/j.enggeo.2015.05.017

Collins, B.D., Stock, G.M., 2016. Rockfall triggering by cyclic thermal stressing of exfoliation fractures. Nat. Geosci. 9, 395–400. https://doi.org/10.1038/ngeo2686

Collins, B.D., Stock, G.M., Eppes, M.C., Lewis, S.W., Corbett, S.C., Smith, J.B., 2018. Thermal influences on spontaneous rock dome exfoliation. Nat. Commun. 9. https://doi.org/10.1038/s41467-017-02728-1

Deprez, M., De Kock, T., De Schutter, G., Cnudde, V., 2020. A review on freeze-thaw action and weathering of rocks. Earth-Sci. Rev. 203, 103143. https://doi.org/10.1016/j.earscirev.2020.103143

Eppes, M.C., Griffing, D., 2010. Granular disintegration of marble in nature: A thermal-mechanical origin for a grus and corestone landscape. Geomorphology 117, 170–180. https://doi.org/10.1016/j.geomorph.2009.11.028

Eppes, M.C., Keanini, R., 2017. Mechanical weathering and rock erosion by climate-dependent subcritical cracking. Rev. Geophys. 55, 470–508. https://doi.org/10.1002/2017RG000557

Eppes, M.C., McFadden, L.D., Wegmann, K.W., Scuderi, L.A., 2010. Cracks in desert pavement rocks: Further insights into mechanical weathering by directional insolation. Geomorphology 123, 97–108. https://doi.org/10.1016/j.geomorph.2010.07.003

Eppes, M.-C. (Missy), 2022. Mechanical Weathering: A Conceptual Overview. Treatise Geomorphol. 30–45. https://doi.org/10.1016/b978-0-12-818234-5.00200-5

Frayssines, M., Hantz, D., 2006. Failure mechanisms and triggering factors in calcareous cliffs of the Subalpine Ranges (French Alps). Eng. Geol. 86, 256–270. https://doi.org/10.1016/j.enggeo.2006.05.009

Galeandro, A., Doglioni, A., Simeone, V., Šimůnek, J., 2014. Analysis of infiltration processes into fractured and swelling soils as triggering factors of landslides. Environ. Earth Sci. 71, 2911–2923. https://doi.org/10.1007/s12665-013-2666-7

Gasc-Barbier, M., Merrien-Soukatchoff, V., Genois, J.-L., Mougins, C., Azémard, P., 2023. 10 Years of Thermo-Mechanical Monitoring of Rock Columns - Les Chandelles De l'Escalette, France. Presented at the 15th ISRM Congress, OnePetro.

Preprint not peer reviewed

This preprint research paper has not been peer reviewed. Electronic copy available at: https://ssrn.com/abstract=4743392

Gasc-Barbier, M., Merrien-Soukatchoff, V., Virely, D., 2021. The role of natural thermal cycles on a limestone cliff mechanical behaviour. Eng. Geol. 293, 106293. https://doi.org/10.1016/j.enggeo.2021.106293

Gasc-Barbier, M., Virely, D., Guittard, J., 2015. Thermal fatigue in rocks- la roque-gageac' case study, in: 13th ISRM International Congress of Rock Mechanics.

Gischig, V., Moore, J.R., Evans, K.F., Loew, S., 2010. Seasonal changes of rock mass deformation rate due to thermal effects at the Randa rock slope instability, Switzerland. Geol. Act. Deleg. Pap. 11th Congr. Int. Assoc. Eng. Geol. Environ. Auckl. Aotearoa 5–10.

Grøneng, G., Christiansen, H.H., Nilsen, B., Blikra, L.H., 2011. Meteorological effects on seasonal displacements of the Åknes rockslide, western Norway. Landslides 8, 1–15. https://doi.org/10.1007/s10346-010-0224-x

Guerin, A., Jaboyedoff, M., Collins, B.D., Stock, G.M., Derron, M.H., Abellán, A., Matasci, B., 2021. Remote thermal detection of exfoliation sheet deformation. Landslides 18, 865–879. https://doi.org/10.1007/s10346-020-01524-1

Gunzburger, Y., Merrien-Soukatchoff, V., 2011. Near-surface temperatures and heat balance of bare outcrops exposed to solar radiation. Earth Surf. Process. Landf. https://doi.org/10.1002/esp.2167

Gunzburger, Y., Merrien-Soukatchoff, V., Guglielmi, Y., 2005. Influence of daily surface temperature fluctuations on rock slope stability: Case study of the Rochers de Valabres slope (France). Int. J. Rock Mech. Min. Sci. 42, 331–349. https://doi.org/10.1016/j.ijrmms.2004.11.003

Hall, K., 1999. The role of thermal stress fatigue in the breakdown of rock in cold regions. Geomorphology 31, 47–63. https://doi.org/10.1016/S0169-555X(99)00072-0

Hall, K., Thorn, C., Sumner, P., 2012. On the persistence of "weathering." Geomorphology 149–150, 1–10. https://doi.org/10.1016/j.geomorph.2011.12.024

Hall, K., Thorn, C.E., 2014. Thermal fatigue and thermal shock in bedrock: An attempt to unravel the geomorphic processes and products. Geomorphology 206, 1–13. https://doi.org/10.1016/j.geomorph.2013.09.022

Iverson, Richard.M., 2000. Landslide triggering by rain infiltration. Water Ressour. Res. 36, 1897–1910.

Krähenbühl, R., 2004. Temperatur und Kluftwasser als Ursachen von Felssturz. Bull. Fuer Angew. Geol. 9, 19–35. https://doi.org/10.5169/seals-224989

Marmoni, G.M., Fiorucci, M., Grechi, G., Martino, S., 2020. Modelling of thermo-mechanical effects in a rock quarry wall induced by near-surface temperature fluctuations. Int. J. Rock Mech. Min. Sci. 134, 104440. https://doi.org/10.1016/j.ijrmms.2020.104440

Matsuoka, N., 2008. Frost weathering and rockwall erosion in the southeastern Swiss Alps: Long-term (1994-2006) observations. Geomorphology 99, 353–368. https://doi.org/10.1016/j.geomorph.2007.11.013

Matsuoka, N., 2001. Direct observation of frost wedging in alpine bedrock. Earth Surf. Process. Landf. 26, 601–614. https://doi.org/10.1002/esp.208

McKay, C.P., Molaro, J.L., Marinova, M.M., 2009. High-frequency rock temperature data from hyper-arid desert environments in the Atacama and the Antarctic Dry Valleys and implications for rock weathering. Geomorphology 110, 182–187. https://doi.org/10.1016/j.geomorph.2009.04.005

Merrien-Soukatchoff, V., Gasc-Barbier, M., 2023. The Effect of Natural Thermal Cycles on Rock Outcrops: Knowledge and Prospect. Rock Mech. Rock Eng. 56, 6797–6822. https://doi.org/10.1007/s00603-023-03420-1

Mufundirwa, A., Fujii, Y., Kodama, N., Kodama, J. ichi, 2011. Analysis of natural rock slope deformations under temperature variation: A case from a cool temperate region in Japan.

This preprint research paper has not been peer reviewed. Electronic copy available at: https://ssrn.com/abstract=4743392

Cold Reg. Sci. Technol. 65, 488–500. https://doi.org/10.1016/j.coldregions.2010.11.003
Racek, O., Balek, J., Loche, M., Vích, D., Blahůt, J., 2023. Rock Surface Strain In Situ Monitoring Affected by Temperature Changes at the Požáry Field Lab (Czechia). Sensors 23, 2237. https://doi.org/10.3390/s23042237
Racek, O., Blahut, J., Hartvich, F., 2021. Observation of the rock slope thermal regime, coupled with crackmeter stability monitoring: Initial results from three different sites in Czechia (central Europe). Geosci. Instrum. Methods Data Syst. 10, 203–218. https://doi.org/10.5194/gi-10-203-2021
Ravaji, B., Alí-Lagoa, V., Delbo, M., Wilkerson, J.W., 2019. Unraveling the Mechanics of Thermal Stress Weathering: Rate-Effects, Size-Effects, and Scaling Laws. J. Geophys. Res. Planets 124, 3304–3328. https://doi.org/10.1029/2019JE006019
Regmi, A.D., Yoshida, K., Dhital, M.R., Devkota, K., 2013. Effect of rock weathering, clay mineralogy, and geological structures in the formation of large landslide, a case study from Dumre Besei landslide, Lesser Himalaya Nepal. Landslides 10, 1–13. https://doi.org/10.1007/s10346-011-0311-7
Vargas, E.A., Castro, J.T., Amaral, C., Figueiredo, R.P., 2004. On mechanisms for failures of some rock slopes in Rio de Janeiro, Brazil: thermal fatigue?, in: Landslides: Evaluation and Stabilization/Glissement de Terrain: Evaluation et Stabilisation, Set of 2 Volumes. pp. 1007–1011.
Vargas, E.A., Chavez, E., Gusmao, L., Amaral, C., 2009. Is thermal fatigue a possible mechanism for failure of some rock slope in Rio de Janeiro, Brazil ?, in: ARMA - 43th US Rock Mech Symposium. Asheville.
Virely, D., Gasc-Barbier, M., Merrien-Soukatchoff, V., 2021. More than eleven years of temperature and displacements recorded on and in a limestone cliff: Dataset. Data Brief 39, 107568. https://doi.org/10.1016/j.dib.2021.107568

Annexes

A1- photos of all sensors on site.

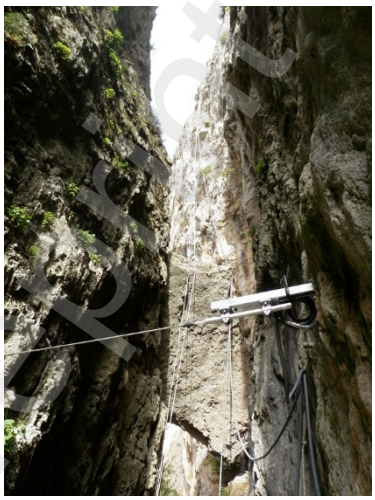

H1

B2

Preprint not peer reviewed

This preprint research paper has not been peer reviewed. Electronic copy available at: https://ssrn.com/abstract=4743392

H3

B4

H5

B6

H7

B8-V8

Preprint not peer reviewed

This preprint research paper has not been peer reviewed. Electronic copy available at: https://ssrn.com/abstract=4743392

H9 (upper view)

B10

690
691
692
693

Preprint not peer reviewed

This preprint research paper has not been peer reviewed. Electronic copy available at: https://ssrn.com/abstract=4743392

694 A2- Temperature recording on all sensors. Weeks' mean (dots: H: green, B: red),
695 maximum and minimum (error bar: H: yellow, B: blue).

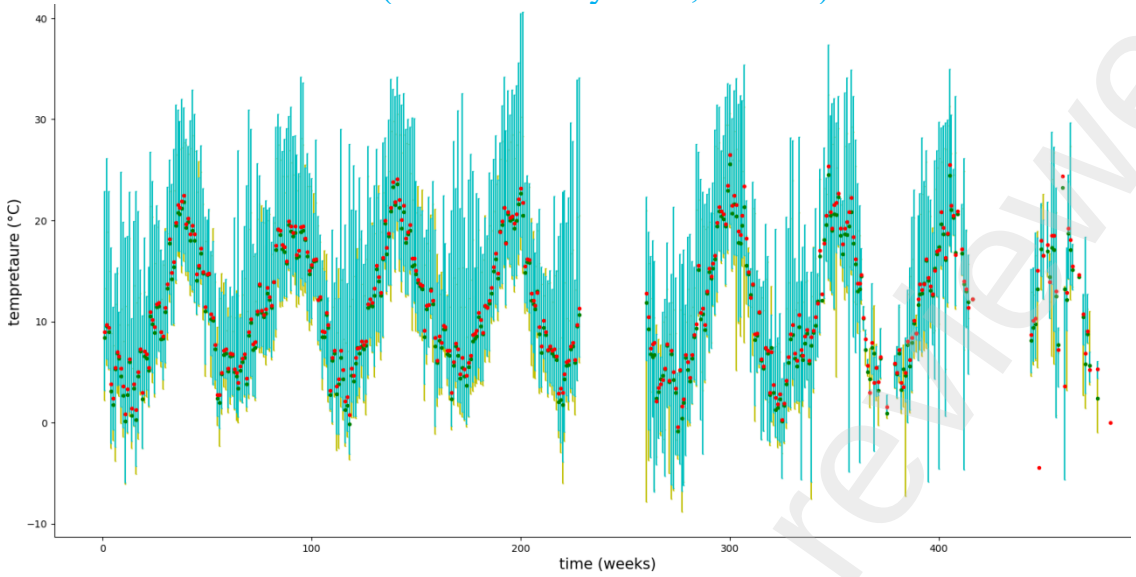

696
697 H1B2

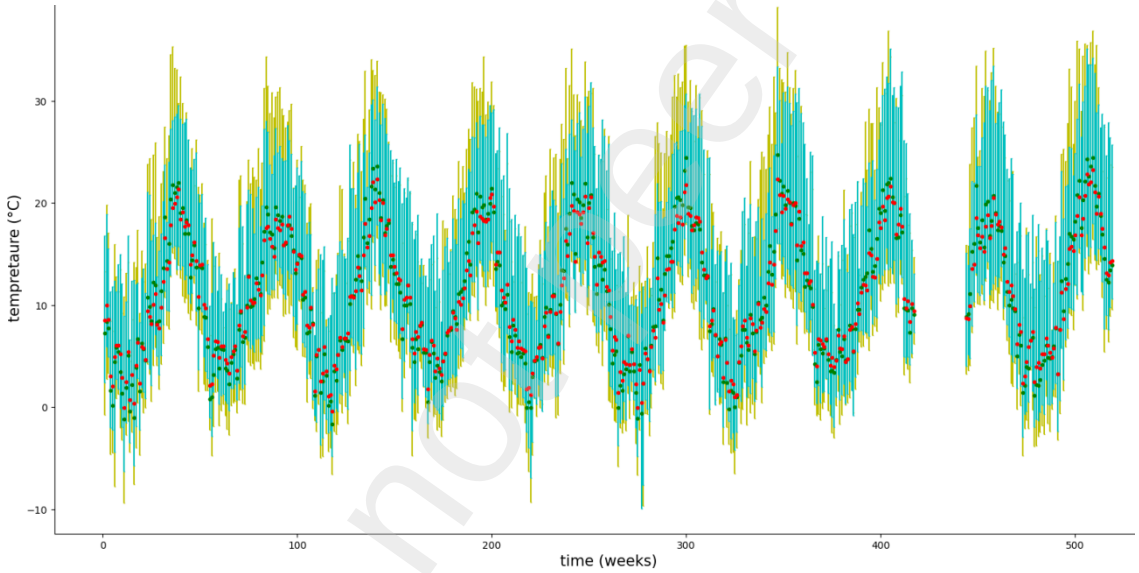

698
699 H3B4

Preprint not peer reviewed

This preprint research paper has not been peer reviewed. Electronic copy available at: https://ssrn.com/abstract=4743392

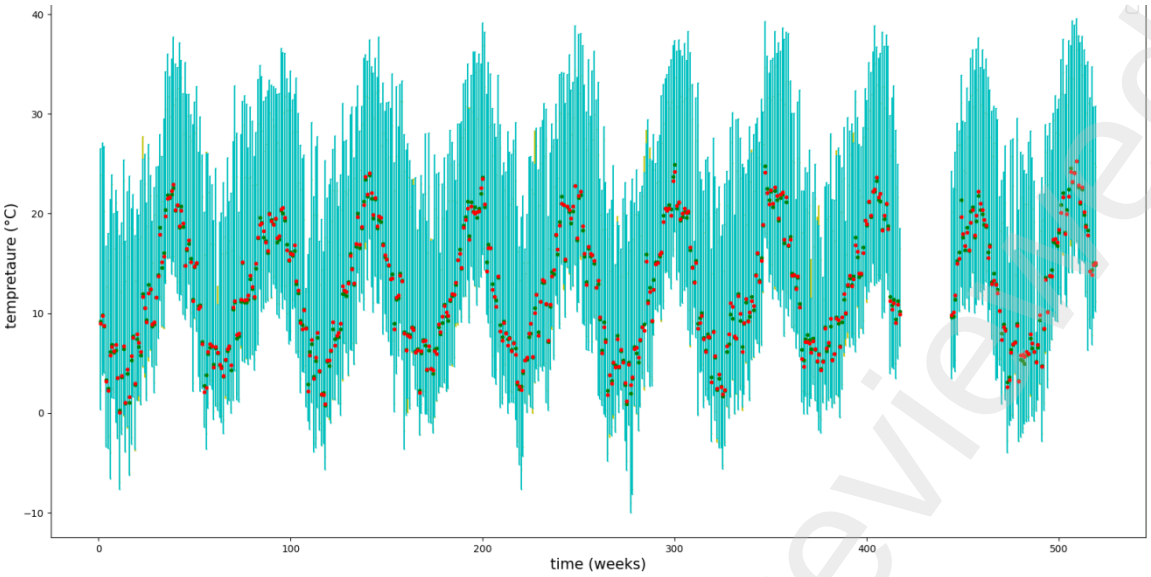

H5B6

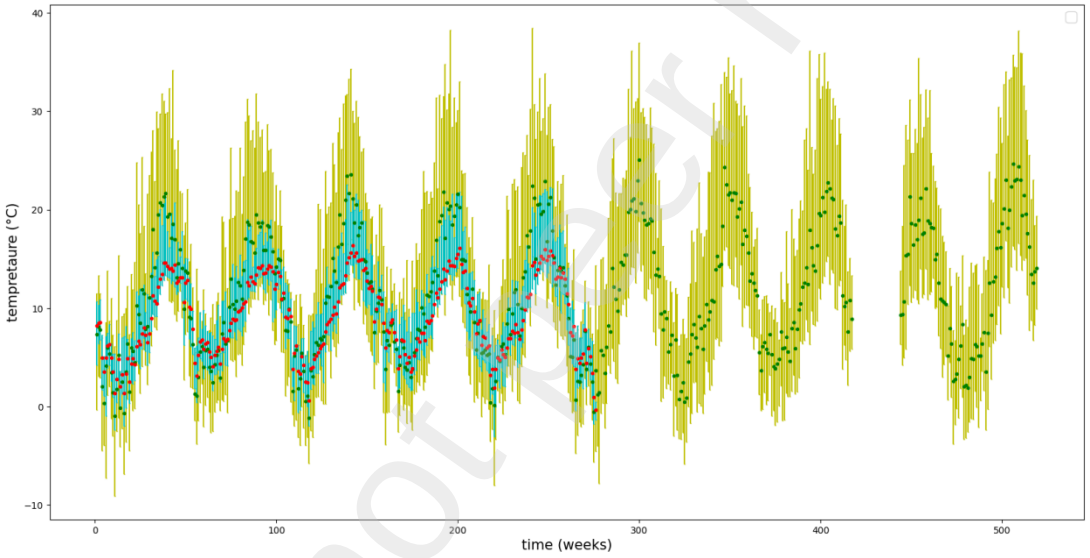

H7B8

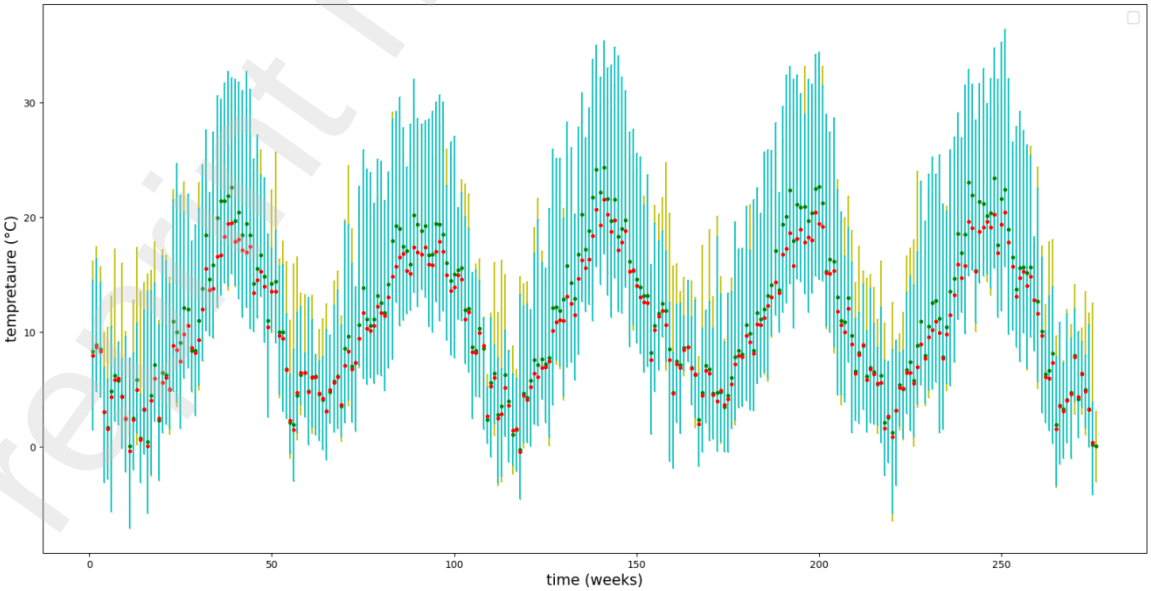

H9B10

This preprint research paper has not been peer reviewed. Electronic copy available at: https://ssrn.com/abstract=4743392

A3- displacement recording on all sensors. Weeks' mean (dots: H: green, B: red), maximum and minimum (error bar: H: yellow, B: blue).

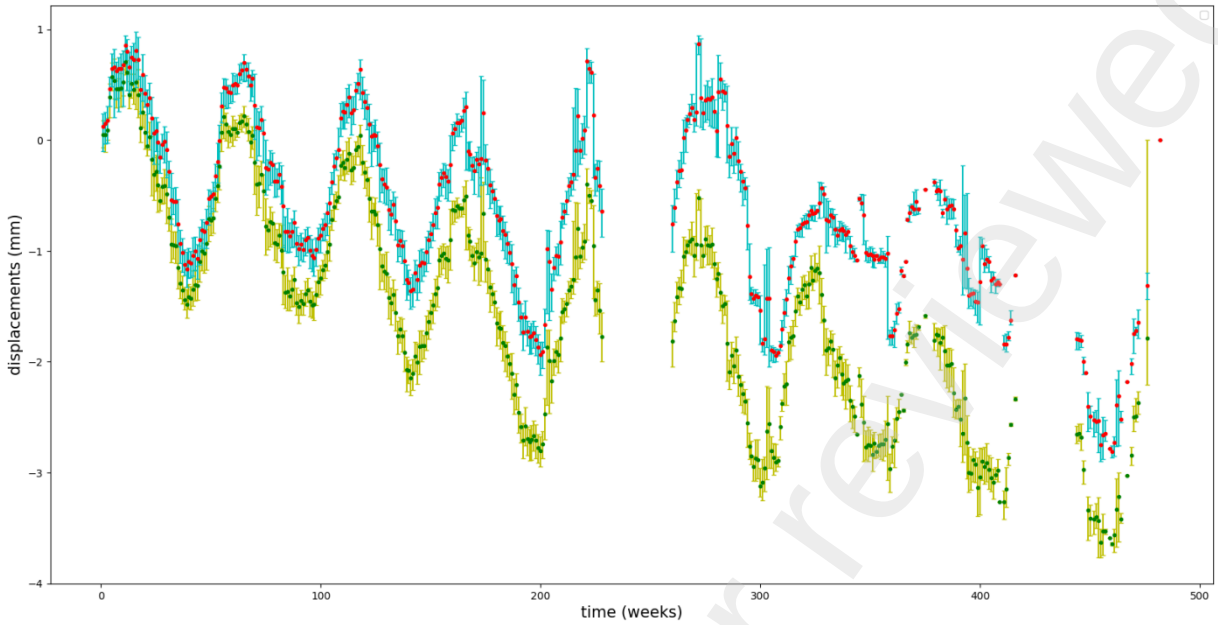

H1B2

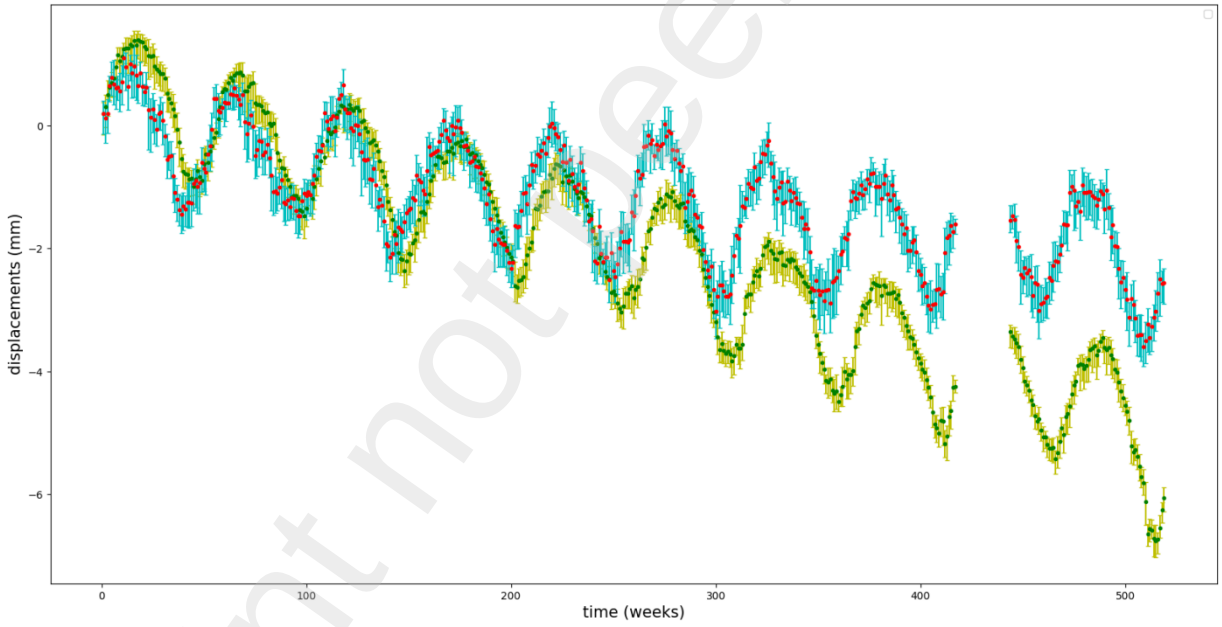

H3B4

Preprint not peer reviewed

This preprint research paper has not been peer reviewed. Electronic copy available at: https://ssrn.com/abstract=4743392

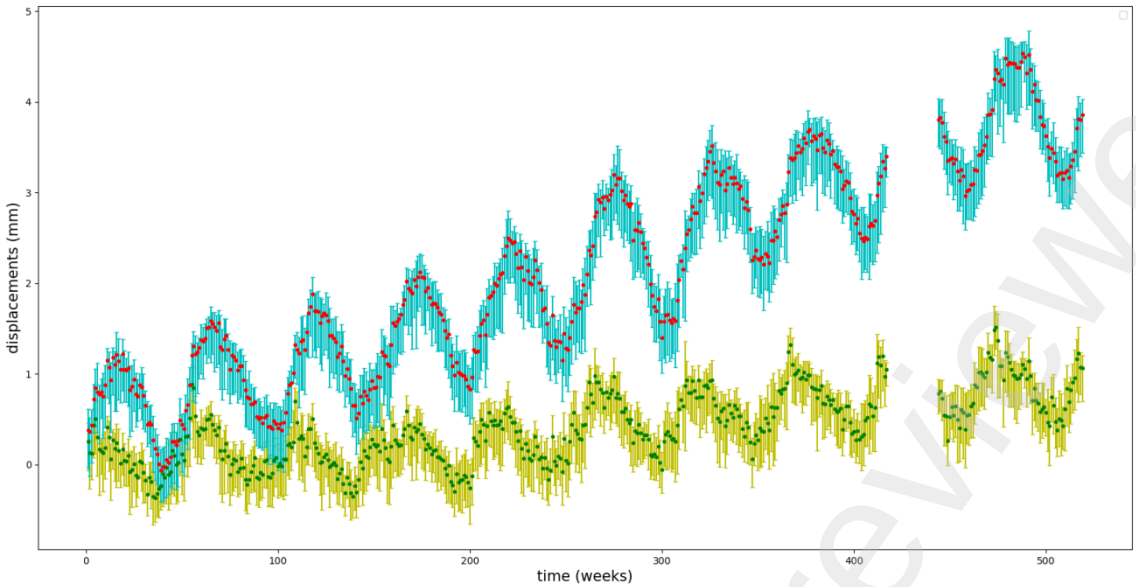

712
713 H5B6

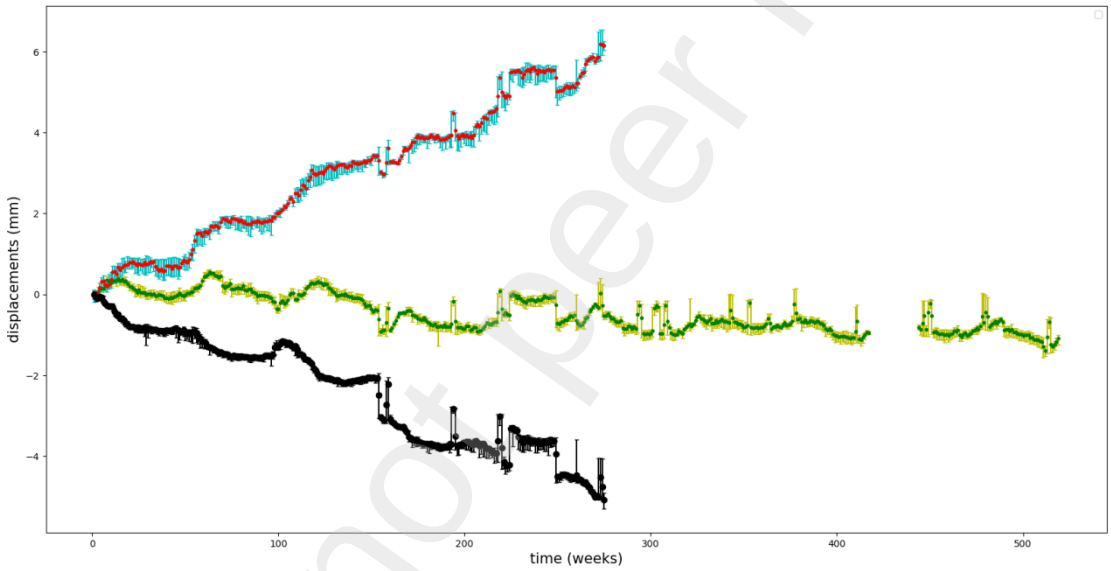

714
715 H7B8V8

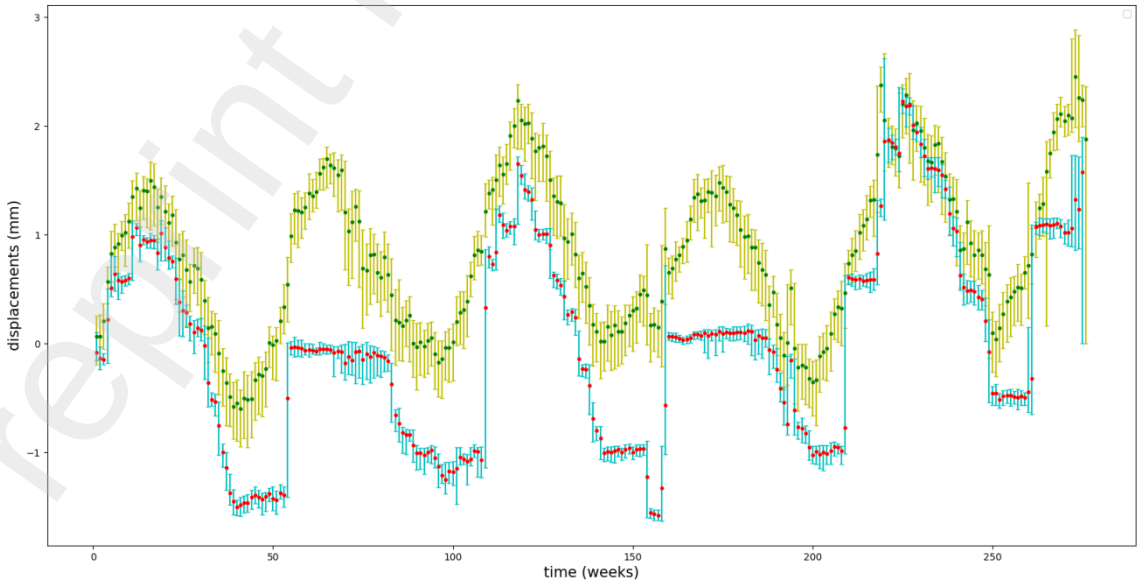

716
717 H9B10

Preprint not peer reviewed

This preprint research paper has not been peer reviewed. Electronic copy available at: https://ssrn.com/abstract=4743392

A4- displacement vs temperature curves

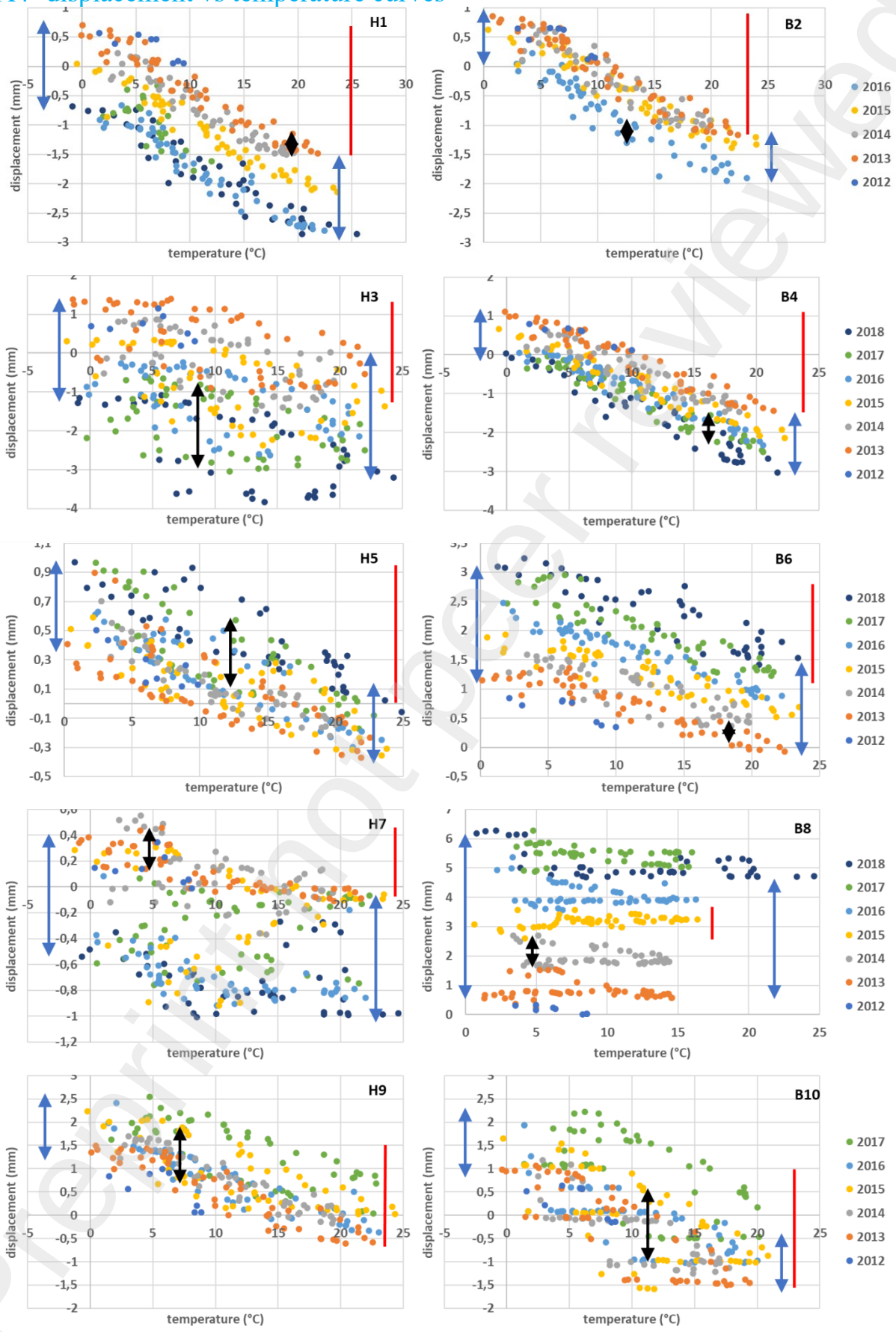

Preprint not peer reviewed

This preprint research paper has not been peer reviewed. Electronic copy available at: https://ssrn.com/abstract=4743392